General Response: We thank the Referee for your helpful comments. We have addressed all comments and provided point by point response below. The revised manuscript is presented in below Response

This study investigates soot mixing states mainly using a transmission electron microscope (TEM) in China and Japan. They collected samples by following the aging of an air plume during a dust event and found changes of soot mixing states as the plume aged. Their findings will be an interesting case study to follow the soot aging in an ambient atmosphere and a heavily polluted area. As the soot aging process is of interest for an understanding of their climate influences through the accurate estimates of soot lifetime and optical properties, their result will have contributions to the climate prediction. However, I have a list of concerns regarding their discussion and interpretations of their results. A major concern is that the many discussion regarding T3 samples (and Type 3 particle) was based only on a particle shown in Fig. 3 d. The authors also try to have a general model based on the one-particle observation; a better statistic is necessary here. Please see the specific comments for more suggestions.
Answer: We appreciated the Referee#1's comments which significantly improve the quality of the manuscript. We carefully answer them one by one as below. The modifications were highlighted in red in the revised manuscript.

1. Line 108-110: from 1 min to 10 min: I see only 1 to 2 min in Table S1.
Answer: Sorry for the misunderstanding. The "1 min to 10 min" is the usual collection time for samples in our overall campaign, but for the dust event samples, the duration is "1 to 2 min". This mistake is corrected in the manuscript.

2. Line 113 (and 86): TEM has been defined as "transmission electron microscopy" in line 86, whereas it is defined as "transmission electron microscope" here. Please be consistent.
Answer: The "transmission electron microscope" has been revised to "transmission electron microscopy".

3. Section 2.5 Line 160-162: It is unclear how the Eq. 3 is used to obtain α and ka here.
Answer: Eq. 3 is used to obtain the overlap parameter (δ). Then the overlap parameter (δ) can be used to acquire α and ka based on Figure 6. in Oh and Sorensen (1997). More detailed information was added in the revised manuscript: "The values of α and ka in Equation 2 depend on the overlap parameter (δ) calculated using Equation 3. Then δ can be used to obtain α and ka based on Fig. 6. in Oh and Sorensen (1997).".

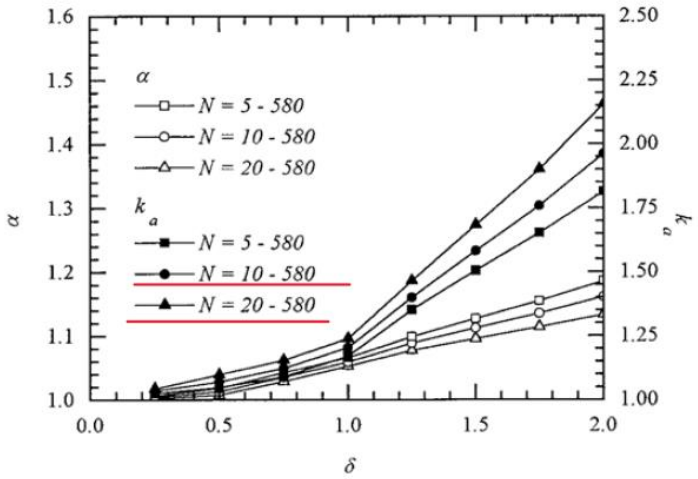

FIG. 6. The parameters α and k_a of Eq. [12] versus overlap parameter for three different fit ranges in N, the number of monomers per cluster.

Figure cited from Oh and Sorensen (1997)

4. Line 180-183: How were the cold front arrival times defined? I do not see a clear change at the time of the arrival in Figures S3-5. As the timing is used to evaluate soot aging time, please make them specific. Why did the authors use Beijing time instead of UTC? As the local time in T3 site is not Beijing time, UTC will be better.

Answer: The local time in T3 site is Japan Standard Time, which is one hour ahead of Beijing Time. In the previous manuscript, we have transformed Japan Standard Time to Beijing Time at T3 to facilitate comparison. We also realize that UTC is much better as the Referee#1 suggested. Therefore, all time used in this paper has been revised to UTC.

The cold front arrival times were defined based on PM concentration in Figure 2 and meteorological data (mainly pressure) in Figures S3-S5. The air behind a cold front is colder and drier than the air in front. When the cold front passes through, the RH and temperature can drop, and the pressure can increase. A clear turning point of pressure is observed in T1 and T2 (Figures S3 and S4), thus we consider this point as the arrival time. For T3, the turning point of pressure is not obvious, but based on the RH and temperature dropping, we still can confirm the arrival time.

We also want to note that the cold front arrival times is not used to evaluate soot aging time, it is only used to confirm the time when the sampling site starts to be influenced by the dust storm. The aging time is obtained from the backward trajectories in Figure 1.

5. Line 196-198: The dust distribution and back-trajectory model in Fig. 1 indicates that the Dust samples at T3 site are not from the dust plume. On 8:00 18 March in Fig. 1, the edge of the dust plume was 18 and 24 hours ahead for the Dust 1 and 2 sampling at T3 site, respectively. Thus, the dust should arrive between 2:00-8:00 19 March at T3 site, whereas the samplings were done at 23:16, 18 March and 6:36, 19 March. At least, the sentence "together verified that the dust storm event" is not valid, unless I miss something. Figure S2 may be helpful, but I cannot see details in the figure. I recommend rechecking the modeling data and showing robust data to prove the dust arrival before the sampling at T3 site. TEM data of dust particles from the T3 site samples may be useful.

Answer: There might be some misunderstanding to interpret the Figure 1. We cannot define the arrival time based on the dust plume (yellow shadow) and backward trajectories. In fact, the intersections between the dust plume and backward trajectories are meaningless. The Dust 1 and 2 samplings were done at 15:16 and 22:36, 18 March (UTC). Therefore, 18 and 24 hours ahead of Dust 1 and 2 is 21:16 and 22:36, 17 March. This is even not the time of the dust plume we present in Figure 1 (00:00, 18 March).

The cold front arrival time was defined based on PM concentration and meteorological data as mentioned in Comment #4.

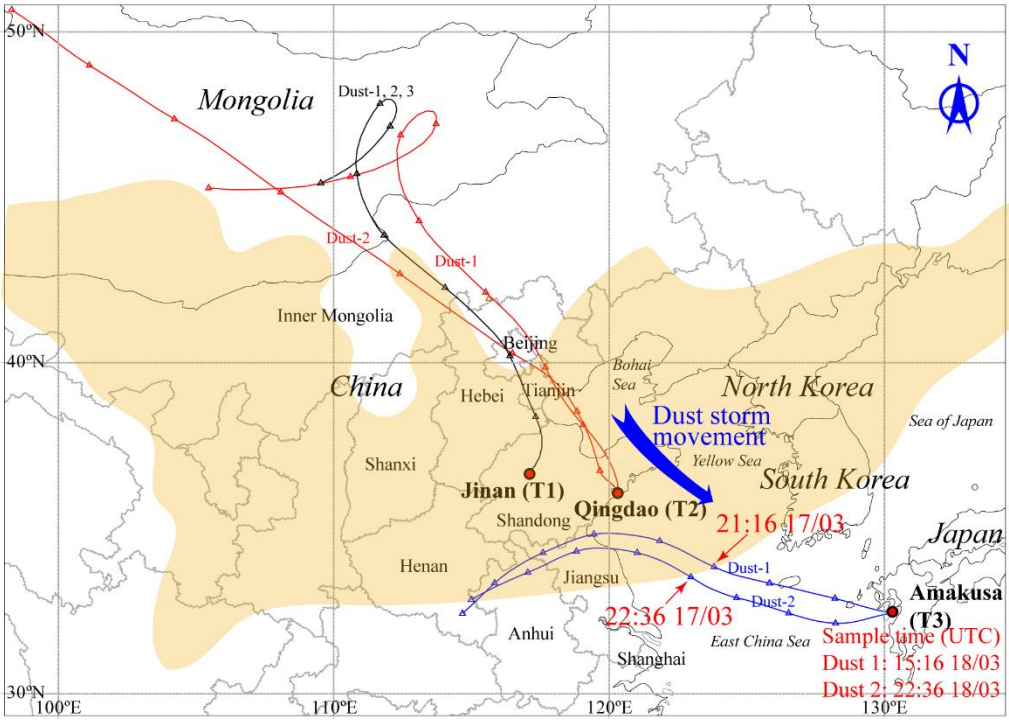

6. Line 205-208: It is surprising that the dust samples have so many soot particles. Are there so many dust particles as well together with soot particles? TEM images with low-magnification showing more particles, including soot and dust, will be helpful to have an idea of how such a large number of soot particles occur in the dust samples.

Answer: We found some but not many dust particles that mixed with soot particles in T3 site. A low-magnification TEM image of T3 is added in the manuscript (Figure 7).

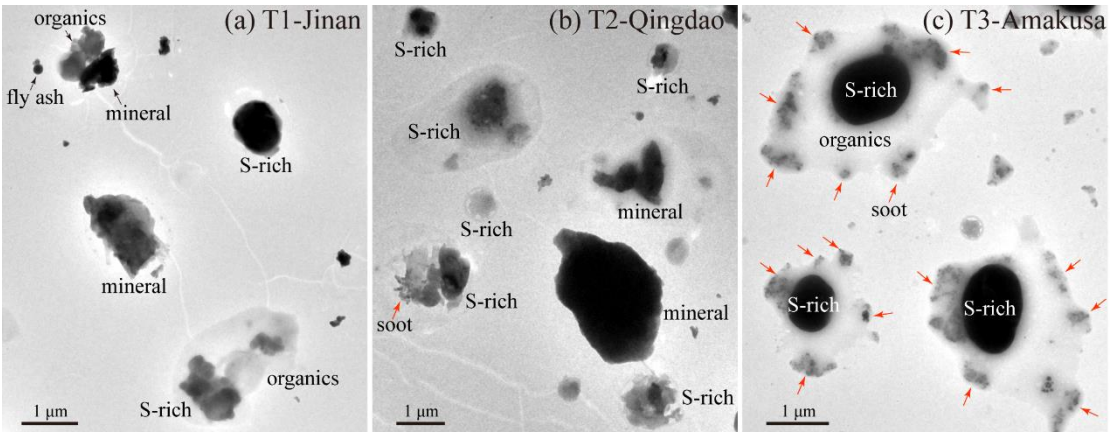

Figure 7. Low-magnification TEM images at T1, T2, and T3.

7. Line 223-224: Do coagulations between soot particles and others contribute to the "partially embedded soot" formation?
Answer: Yes, it is.

8. Line 237-242: When the soot particles are fully coated, such as aged samples at T3, the deposition efficiency of fully embedded soot-bearing particles may not differ from those without soot. I assume that the increase of the number fraction of soot-bearing particles is simply due to an increase of mixing state index as aging (Riemer and West, 2013; Healy et al., 2014), but more discussion will be useful here.
Answer: Thanks for the valuable suggestion. We add the discussion that the increase of mixing state index during soot aging could lead to the number fraction increase (Line 247-251): "Moreover, the number fraction increase of soot-bearing particles also could be attributed to the increase of mixing state index (the metric to quantify the population mixing state, ranging from 0 for a completely external mixture to 1 for a completely internal mixture) as aging during transport (Riemer and West, 2013;Healy et al., 2014)."

9. Line 247-254 and 258-259: I suggest adding TEM images, including many soot particles having high or low fractal dimensions, so that readers visually see the compaction of soot particles as age.
Answer: The D_f in this paper was acquired using statistical method (slope in Figure 5), the method cannot provide D_f value for one single soot particle. Here, we provide model simulated soot particles with different D_f to represent different soot morphology. The new figure should be helpful for the readers to visually understand the soot compaction.

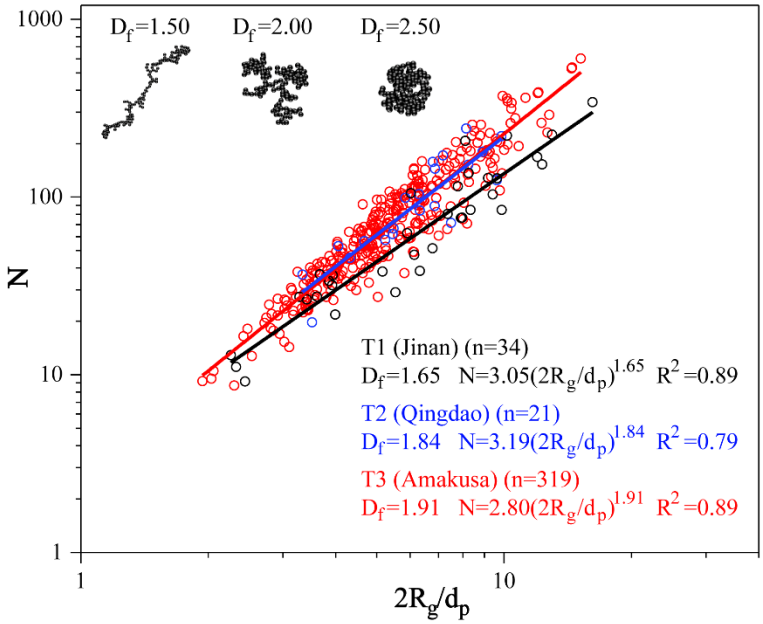

Figure 5. Fractal dimension of soot-bearing particles at the three sampling sites. The parameter n in parentheses represents the total number of soot particles analyzed for each site to calculate Df and kg.

10. Line 263-265: It is unclear how the Dcore was obtained. As soot particles have a fractal structure, Dp and Dcore should have different relations in Fig. S6. Please explain the methodology.

Answer: For soot particles with fractal shape, we manually draw an interpolated polygon to fully cover the edge of soot particles (see figures below). Our iTEM software could obtain the area of this polygon based on our manual drawing, and further convert the area to the equivalent circle diameter (ECD) of soot particles.

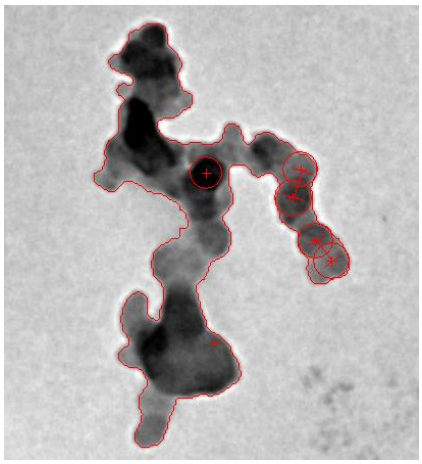

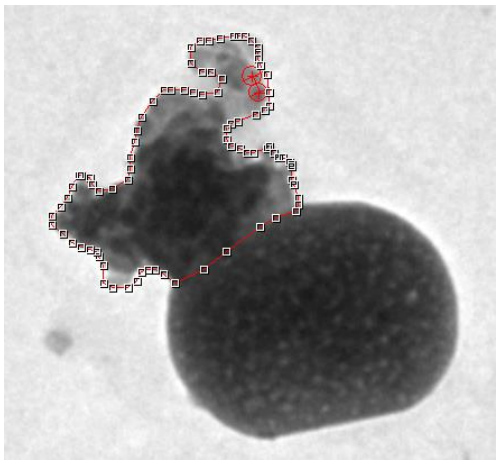

The relations of ECD and EVD in Figure S6 are obtained for sulfur-rich particles. During sample collection, the impaction could lead to morphological change (see figure below). The particle ECD from TEM is larger than its diameter in the air. Thus, we convert S-rich particles' ECD to EVD to acquire the Dp.

But the size of soot is less affected by the impaction. We apply the ECD of soot as the Dcore.

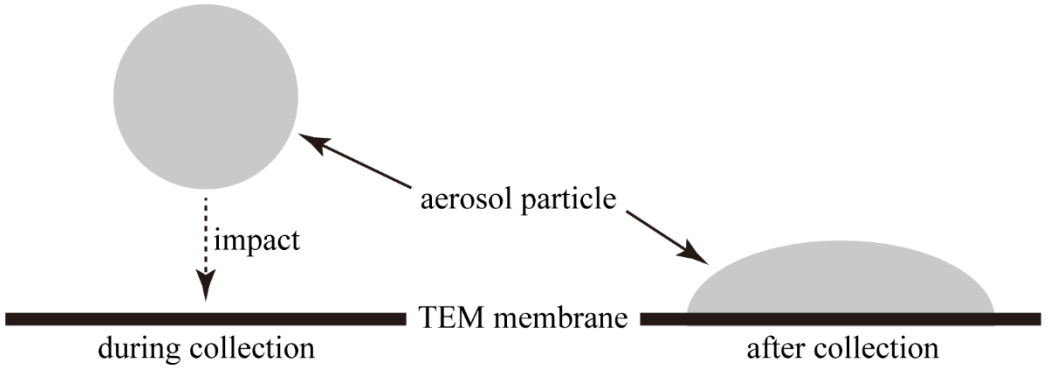

About the conversion from ECD to EVD, our previous studies have quantify the secondary sulfate particles (Chen et al., 2017; Zhang et al., 2020). The same method was adopted in this study.

11. Line 307-327: The discussion in this paragraph based on only one particle (Fig. 3d), and it is difficult to have a general conclusion. I suggest showing more particle images or adding statistics of the fraction having particles with phase separation or tiny soot particles. I also question how the fractal dimensions or other parameters were obtained from the scattered soot particles.

Answer: We add the low-magnification TEM images of T1, T2, and T3 as suggested in Comment #15. More particles with phase separation and tiny soot are shown in the T3 image

(Figure 7).

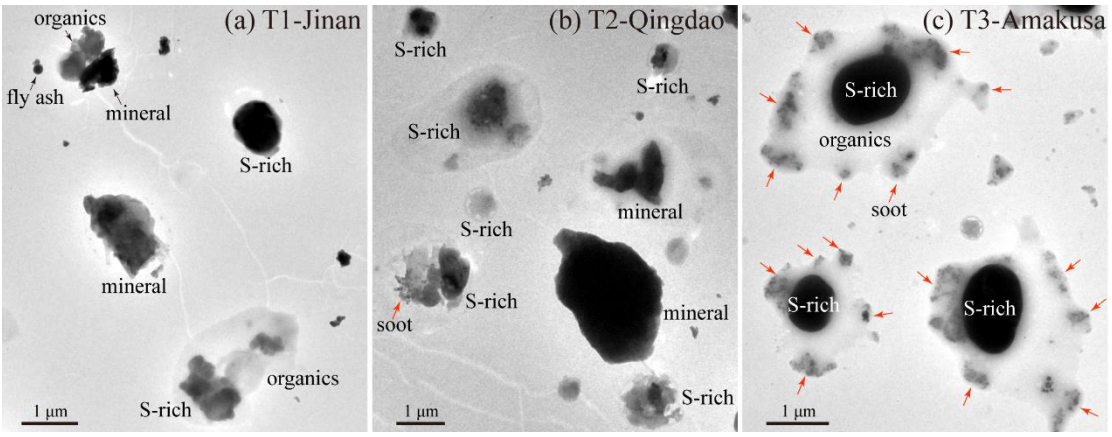

Figure 7. Low-magnification TEM images at T1, T2, and T3.

The fractal dimensions and other parameters of the scattered soot particles were acquired same as other soot particles. We manually draw a interpolated polygon to fully cover the edge of soot particles and obtain data from our iTEM software.

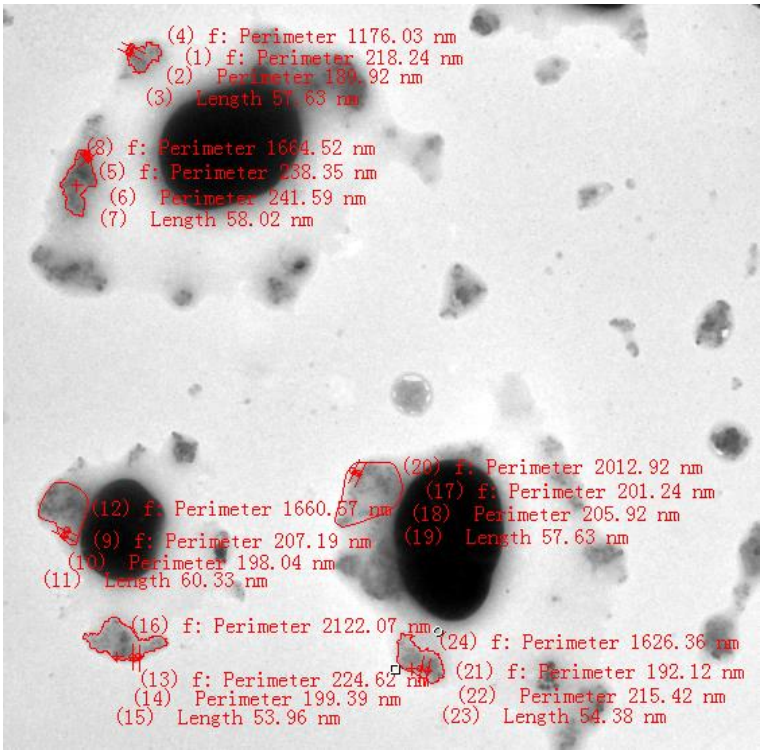

12. Line 326-330: I do not see any evidence of cloud-aqueous process discussed here. Are there any cloud in the dust plume? How do "the cloud-aqueous process and the phase separation of organic and sulfate components in the soot-bearing particles likely break the chain-like soot" happen? Do the "the cloud-aqueous process and the phase separation" make soot compact or scatter? Careful discussions should be provided here.

Answer: We agree with the referee that the expression in this sentence is not precise. Especially we do not have solid proof for the cloud process.

The aqueous process could be a possible reason for the formation of scattered soot in coating. Secondary aerosol particles begin to acquire aqueous shells at RH 60% (Sun et al.,

2018). The high RH in marine air could lead to secondary aerosols change from a solid to liquid phase. Therefore, we propose that the aqueous process and the phase separation of organic and sulfate likely is the reason of soot in the coating.

As for the tiny size soot in the coating, there is no previous studies to report the scattered tiny soot phenomenon. Here we proposed possible reasons for this: (1) the aqueous process and the phase separation break the chain-like soot; (2) soot particle with smaller size have a longer lifetime and could be transported over longer distances. From our current knowledge, the second reason has a better chance to explain this. Thus, we revise the corresponding part in the manuscript (Line 337-341): "There is no previous study to report the tiny scattered soot in the organic coating. We proposed a possible reason that soot particle with smaller size have a longer lifetime and could be transported over longer distances. Therefore, the tiny soot particles have more chances to coagulate with preexisting aqueous secondary particles in marine air (Liu et al., 2018)." However, the reason for this requires further work.

13. Line 363-366: The conclusion was obtained only one soot particle. Please show more data or revise the conclusion. It sounds that the conclusion "that the complicated aging processes of individual particles can break the chain-like soot formation" contradicts with soot compaction process. Please have a comment on this.

Answer: Thanks. We seriously consider this comment here. TEM image of particles with phase separation and tiny soot are shown in the T3 image.

The contradicted sentence was deleted from the conclusion to avoid potential misunderstanding.

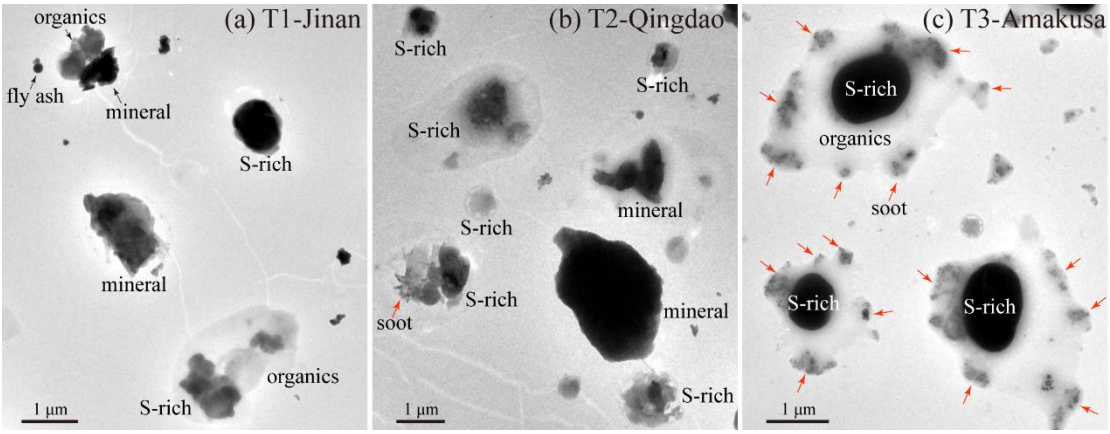

Figure 7. Low-magnification TEM images at T1, T2, and T3.

14. Figure 2: Dust 1 in T2 was collected ahead of the samples in T1. Dust 2 in the T2 was collected only 3 hour ahead of the T3 dust 1 sample. Ideally, if someone wants to compare the aging process, the samples should be collected within the same plume, following the airmass movement. The sampling strategy may cause an influence, and some discussion about the sampling strategy may be helpful.

Answer: Yes, this is the most ideal way to observe the aging process. However we cannot know the precise movement of dust air mass during in-situ sample collection. The influence of dust air mass could last a relatively long time at one site. Therefore, we adopted all the samples collected in the period under the influence of the dust air mass (Figure 2). Thus, even though the samples are not precisely sampled following the air mass movement, the samples could still

represent the characteristics of soot aging. As our prepared study and clear aim, this is the best way to achieve this study.

15. Figure 3: I recommend having more particle images, including low-magnification images from T1, T2, and T3 sites.

Answer: Low-magnification images from T1, T2, and T3 were added in the manuscript (Figure 7).

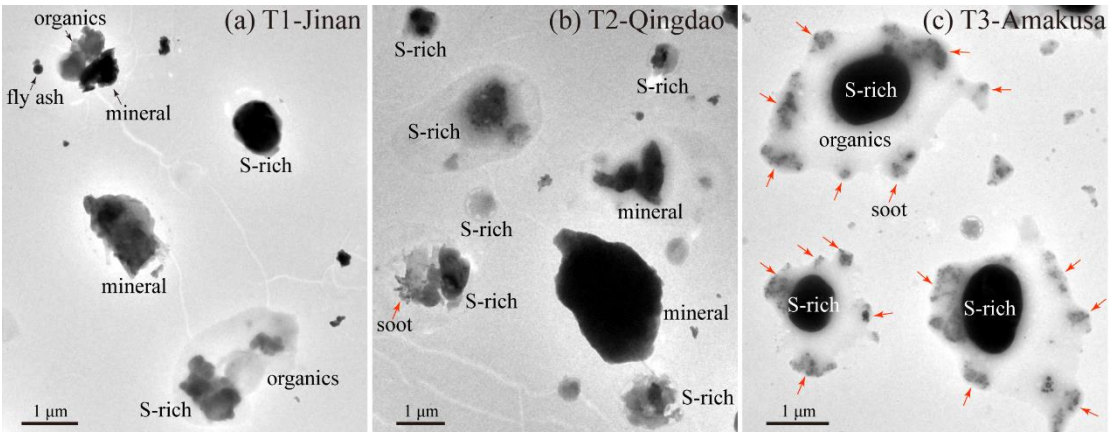

Figure 7. Low-magnification TEM images at T1, T2, and T3.

16. Figures 4 and 5a. The number of analyzed soot particles does not agree between Fig. 4 and 5a (e.g., 80 vs 36). Did the author select soot particles for the analysis in Fig. 5a? If so, how and does the method cause any bias?

Answer: Actually, we did not select soot particles for the D_f analysis in Figure 5. There are some soot particles that can be recognized as soot structure but they are not clear enough to provide necessary data for D_f analysis (mainly in the low-magnification TEM images).

For example, the figure below is not clear any more for D_f analysis, but we can identify this soot from their EDS and morphology. The information still can be used for the statistic in Figure 4.

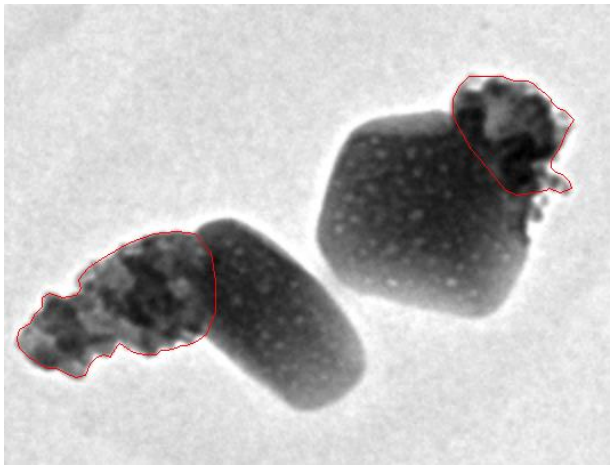

As a result, the soot number in Figure 4 and Figure 5 is not consistent. We can guarantee that we do not occasionally chose soot particles in the sample.

For better description, we add more explanations in the caption of Figure 5: “The inconsistency

of analyzed soot number in Figure 4 and 5 is attributed to the indistinct soot particles in the low-magnification TEM images that can be identified as soot but cannot provide necessary data for Df analysis".

17. Fig. 5b: The error bars are too high to compare the data. What do the bars indicate?
Answer: The error bars indicate the standard deviation. We realize that the average values and error bars are not sufficient to compare the data. Therefore, we replace it with the box plot to clearly show the variation of data. Also, we replace previous aspect ratio with a commonly used morphological descriptor shape factor to better represent soot morphology difference.

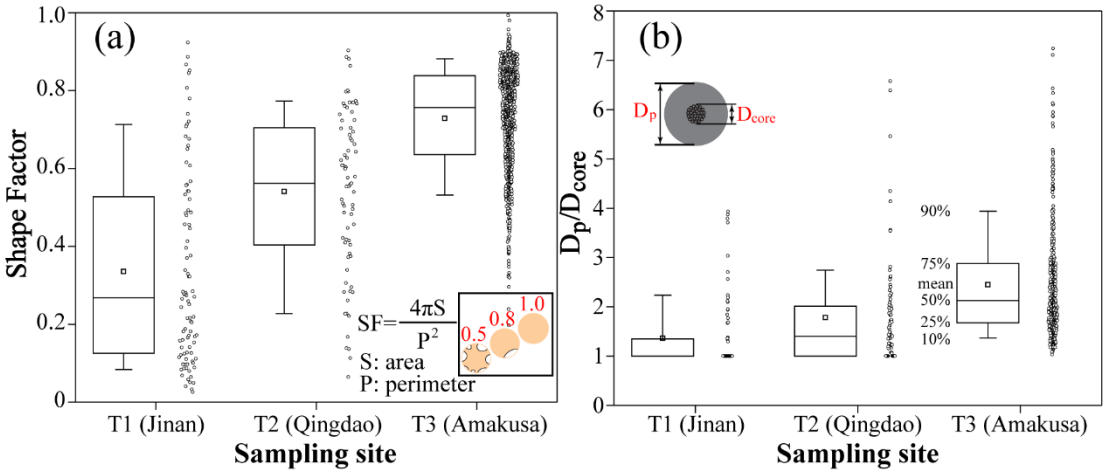

Figure 6. (a) Shape factor of soot-bearing particles at the three sampling sites and (b) the particle-to-soot core diameter ratio (Dp/Dcore).

18. Fig. 6: If there are soot and other emissions at T2, the aging process will be rather complicated, i.e., they should be the mixtures of aged soot and freshly emitted soot. The influence of the emission at T2 should be discussed.
Answer: We agree with the referee that local emissions at T2 could influence the observation of soot aging process. In our study, dust samples at T2 were all collected during the dust storm period. The strong diffusion during the dust storm is not conducive to soot accumulation. Thus, long-range transported soot is still the dominant at T2 among the dust period.
We add more discussion in Line 295-298: "The strong diffusion during the dust storm is not conducive to soot accumulation (Pan et al., 2015). Although local emissions at T2 could interference the observation of soot aging process, long-range transported soot particles were still dominant at T2 during the cold front."

19. Table S1. The wind directions for the samples within the same sampling site vary largely (almost opposite directions (e.g., 121 vs. 358 at T3). The wind direction in Fig S1 at T3 is also complicated. I question if the samples were collected from dust plume. Again, TEM images of dust particles may be helpful.
Answer: The wind directions recorded during our sampling could be considered as the instant wind direction (two minutes maximum, Table S1). This instant direction cannot represent the regional wind. However, the PM concentration, meteorological data, and the dust distribution could provide solid proof for the sample collection in dust plume.

20. Figure S2. It is difficult to see the details.

Answer: We adjusted the arrangement of Figure S2 to make the details more readable.

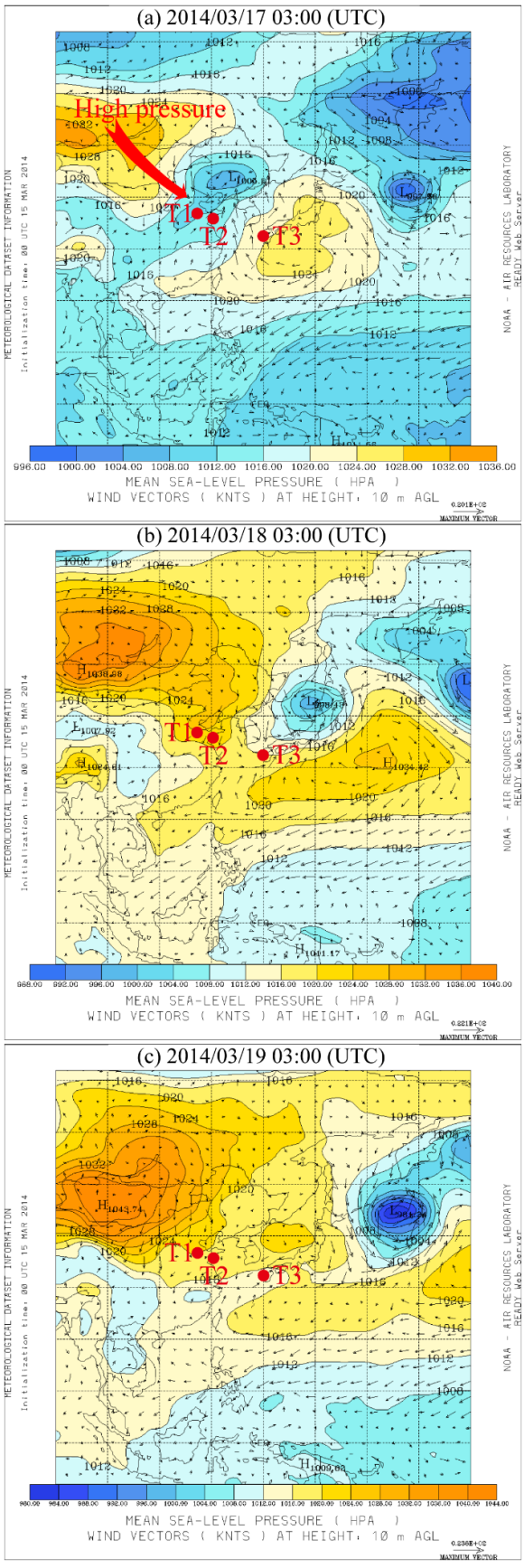

21. Figure S6. Is the plot include soot particles?

Answer: As mentioned in Comment #10, the relations of ECD and EVD in Figure S6 are obtained for sulfur-rich particles.

References:

Healy, R. M., Riemer, N., Wenger, J. C., Murphy, M., West, M., Poulain, L., Wiedensohler, A., O'Connor, I. P., McGillicuddy, E., Sodeau, J. R., and Evans, G. J.: Single particle diversity and mixing state measurements, Atmos. Chem. Phys., 14, 6289–6299, https://doi.org/10.5194/acp-14-6289-2014, 2014.

Riemer, N. and West, M.: Quantifying aerosol mixing state with entropy and diversity measures, Atmos. Chem. Phys., 13, 11423–11439, https://doi.org/10.5194/acp-13-11423-2013, 2013.

Chen, S., Xu, L., Zhang, Y., Chen, B., Wang, X., Zhang, X., et al. (2017). Direct observations of organic aerosols in common wintertime hazes in North China: insights into direct emissions from Chinese residential stoves. *Atmospheric Chemistry and Physics*, *17*(2), 1259-1270. https://doi.org/10.5194/acp-17-1259-2017

Oh, C., & Sorensen, C. M. (1997). The Effect of Overlap between Monomers on the Determination of Fractal Cluster Morphology. *Journal of Colloid and Interface Science*, *193*(1), 17-25. https://doi.org/10.1006/jcis.1997.5046

Sun, J., Liu, L., Xu, L., Wang, Y., Wu, Z., Hu, M., et al. (2018). Key Role of Nitrate in Phase Transitions of Urban Particles: Implications of Important Reactive Surfaces for Secondary Aerosol Formation. *Journal of Geophysical Research: Atmospheres*, *123*(2), 1234-1243. https://doi.org/10.1002/2017JD027264

Zhang, J., Liu, L., Xu, L., Lin, Q., Zhao, H., Wang, Z., et al. (2020). Exploring wintertime regional haze in northeast China: role of coal and biomass burning. *Atmospheric Chemistry and Physics*, *20*(9), 5355-5372. https://doi.org/10.5194/acp-20-5355-2020

General Response: We thank the Referee for your helpful comments. We have addressed all comments and provided point by point response below. The revised manuscript is presented in below Response

The study by Xu et al. investigates the aging of soot particles during Asian dust event. The authors collected samples at three sites and compared soot aging at single particle basis. They mainly used transmission electron microscopy (TEM) to study morphology of soot particles. Several morphological descriptors such as aspect ratio, fractal dimensions are used to quantify morphology of soot particles and they classified mixing state of soot-bearing particles based on their coating thickness. They found that soot particles are compact with highest fractal dimension of soot collected at coastal site (T3) in southwestern Japan. They suggested that compact morphology is due to condensation of secondary coating material and though phase separation at high humidity during transport. The research topic is certainly relevant, but I have several concerns.

Answer: We appreciated the Referee#2's comments which significantly improve the quality of the manuscript. We carefully answer them one by one as below. The modifications were highlighted in red in the revised manuscript.

1. There is not much discussion about the chemical composition of soot-bearing particles. Did you perform any chemical analysis?

Answer: Yes, we applied chemical analysis using an energy-dispersive X-ray spectrometer (EDS). The sulfur-rich and organics are the main component mixed with soot, this has been mentioned in 3.2 and Figure 3. Because soot have typical morphology and only contain C and minor O, therefore we did not have more discussion on it.

2. The backtrajectory analysis is not properly discussed in the manuscript. However, this is key for the dust event discussion. I didn't follow the cold front arrival. The authors should discuss in more detail.

Answer: (1) More discussion about the backward trajectory is added in the manuscript (Line 195-198): "The transport duration from the BTH to T1 and T2 was about 12 hours and 15 hours, respectively. Thus, we estimated that the interval between T1 and T2 was three hours. After passing over T1 and T2, the air masses kept moving southeastward to Japan. The estimated interval between T2 and T3 was 30 hours."

(2) The cold front arrival times is used to confirm the time when the sampling site starts to be influenced by the dust storm. They were defined based on PM concentration in Figure 2 and meteorological data (mainly pressure) in Figures S3-S5. Here we add more description in caption of Figure 2: "The cold front arrival times indicate the time when the sampling site starts to be influenced by the dust storm."

3. What is the relevance of dust storm here? If soot particles are studied during a dust storm, why the authors didn't observe or discuss about mixing of dust and soot particles. The authors should discuss about number fraction of soot particles that are mixed with dust particles and size distribution of both dust and soot particles.

Answer: We appreciate the referee's comments. Soot particles mostly have smaller size <500

nm but dust particles mostly are in larger size (> 2um). Although we observed several dust particles associated with soot particles, the number faction is too small (Figure 7). That is the reason that we did not describe more about the mixture of dust and soot particles. Here we mainly consider the movement of the strong cold front during the dust storm. Here the dramatic high PM10 concentrations during the dust storm can be helpful to confirm the cold front. In light of the primary purpose of this study, we did not focus on the dust particles like our previous studies such as (Li et al., 2016;Li and Shao, 2009).

The size distribution of soot particles is presented in the next comment.

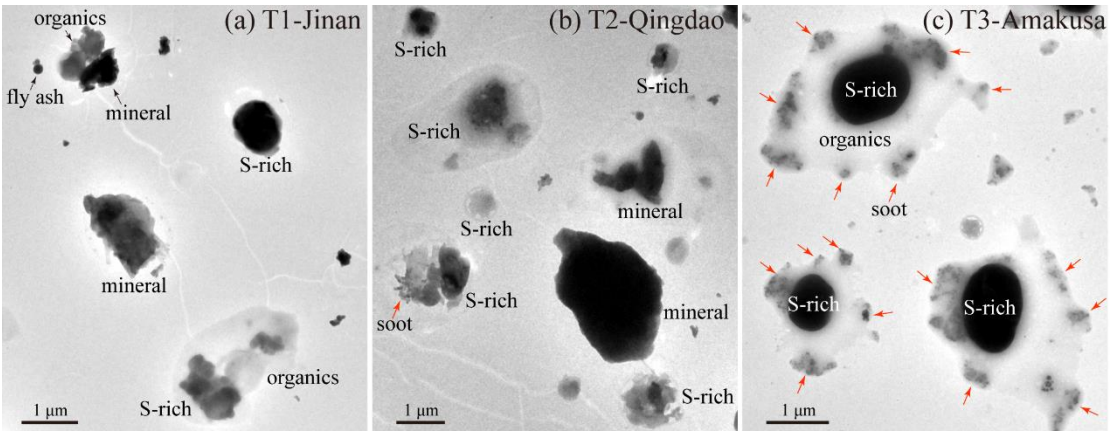

Figure 7. Low-magnification TEM images at T1, T2, and T3.

4. The authors should discuss about the size distribution of three types of soot particles. How did the authors calculate fractal dimension of partially embedded and fully embedded soot particles? For type 3, especially for the fragmented soot ones, it is difficult to measure the required parameters to calculate fractal dimension. They should also provide fractal dimension separately for all three types of soot.

Answer: As the referee's comments, we add more data as below.

(1) The size distribution of soot particles at three sites is provided as follow (Line 273-276): "Size distribution of the soot core indicates a small difference between T1, T2, and T3 during the dust storm period (Figure S9). Thus, the Dp/Dcore increase from T1 to T3 is attributed to the increased coating thickness."

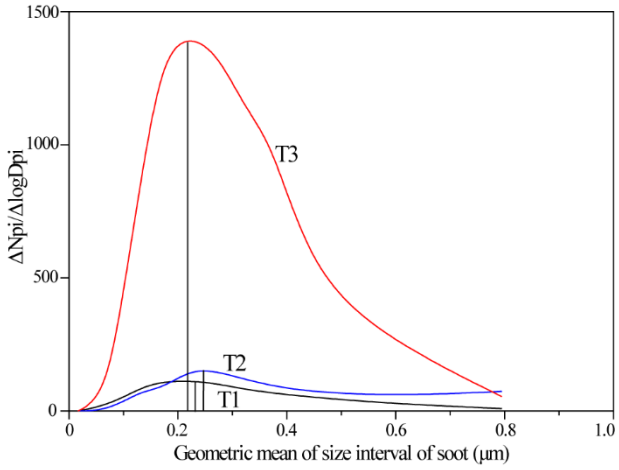

Figure S8. Size distribution of soot core (exclude coating) at T1, T2, and T3.

(2) For soot particles with fractal shape, we manually draw a interpolated polygon to fully cover the edge of soot particles (see figures below). Our iTEM software could obtain the area of this polygon based on our manual drawing, and further convert the area to the equivalent circle diameter (ECD) of soot particles.

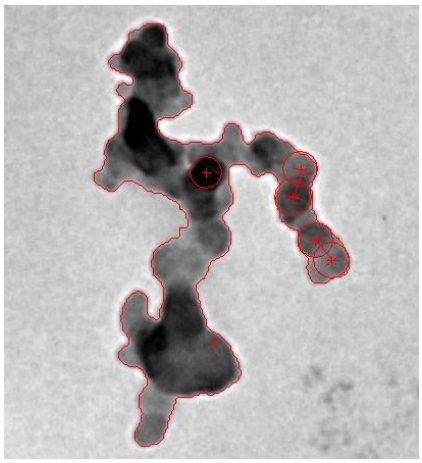

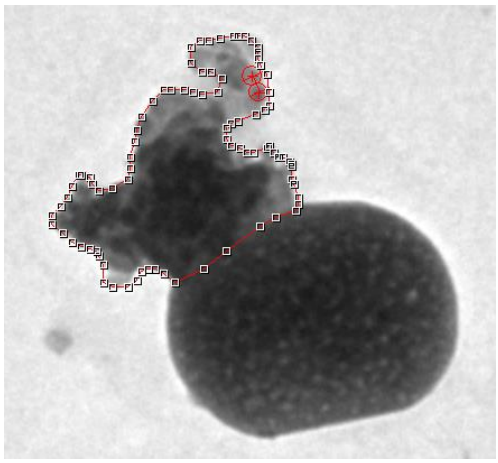

The fractal dimensions and other parameters of the scattered soot particles were acquired same as other soot particles. We manually draw a interpolated polygon to fully cover the edge of soot particles and obtain data from our iTEM software.

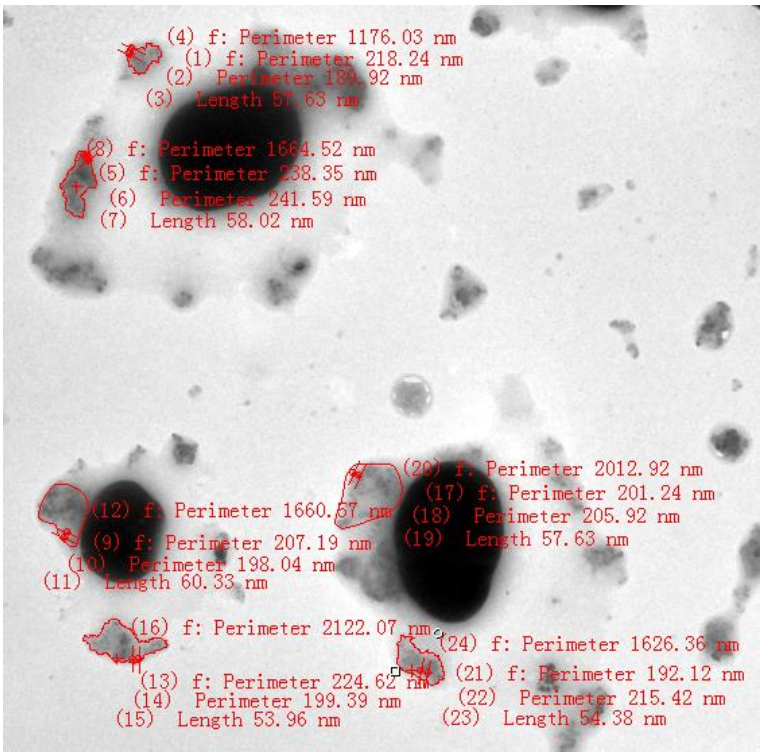

It is true that measuring the required parameters to calculate fractal dimension is difficult, especially in low-magnification TEM images. But, we still can acquire the corresponding parameters from high-resolution TEM images.

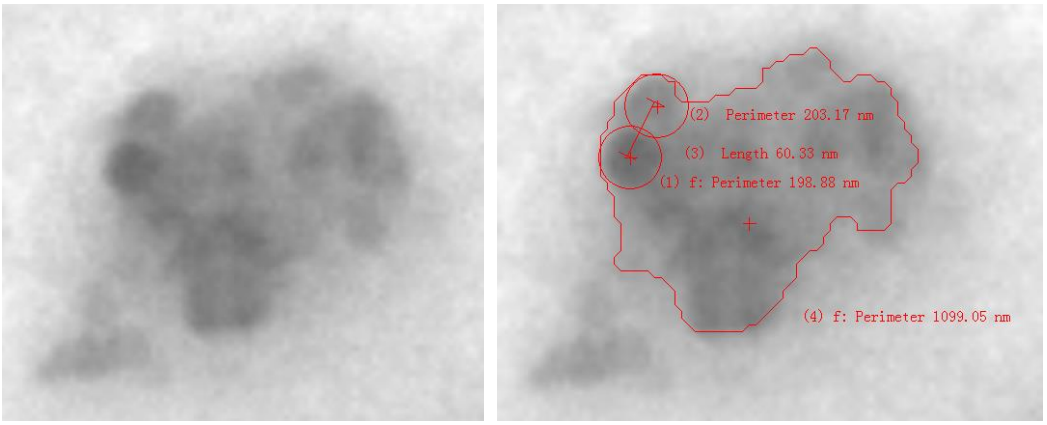

(3) Thanks to Referee's valuable advice, we realized that there was an issue in the D_f analyses. Thus, we recalculated the D_f in Figure 5. However, there are few soot particles at T1 and T2 that can be used for D_f analyses (34 and 21,respectively). We cannnot provide fractal dimension of all three types of soot at T1 and T2. As for T3, we calculate the fractal dimension of partially and fully embeded in the Supporting Information (no fresh soot particle observed at T3).

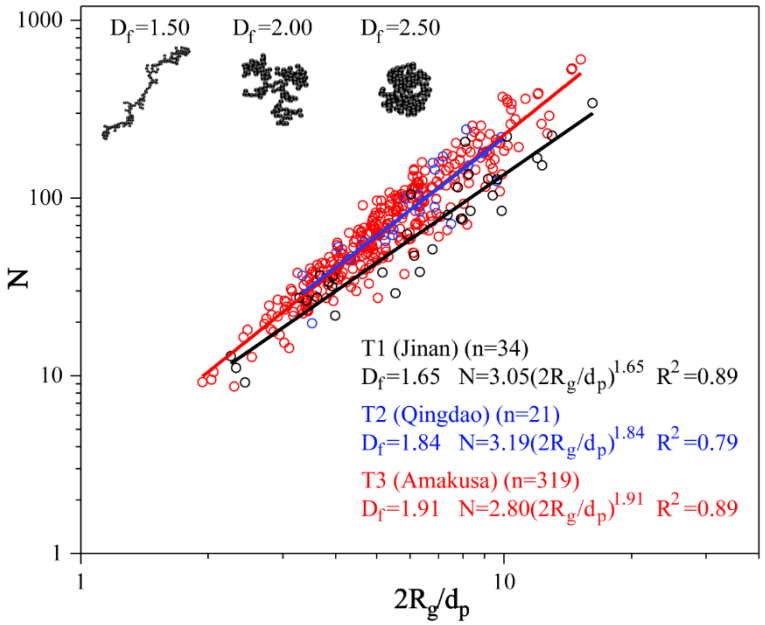

Figure 5. Fractal dimension of soot-bearing particles at the three sampling sites. The parameter n in parentheses represents the total number of soot particles analyzed for each site to calculate Df and kg.

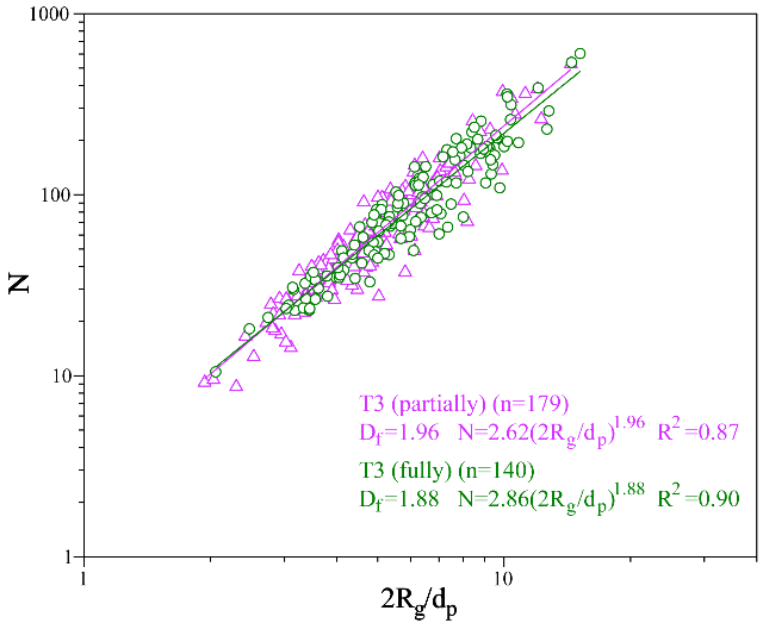

Figure S7. Fractal dimension of partially and fully embedded soot particles at T3 site. It is different to provide fractal dimension of different types of soot at T1 and T2 because of the small number of soot particles at these two sites. The parameter n in parentheses represents the total number of soot particles analyzed for each site to calculate D_f and k_g

5. The discussion about the mixing state configuration needs to be elaborated, like how many soot particles did you observe within individual partially embedded soot particles? How many fragments were observed in type-3 (figure 3d). This information would be useful to understand the aging process and for modeling purposes.

Answer: We provided the frequency of soot fragment number in single soot-bearing particles. More discussion is added in Line 228-229: "Most of partially embedded soot particles include one soot core, only ~ 10% of them contain two soot cores (Figure S7)";

Line 321-323: "More than half of this type of particles contain one or two soot fragments, while 43% of them include more than three soot fragments (Figure S7)."

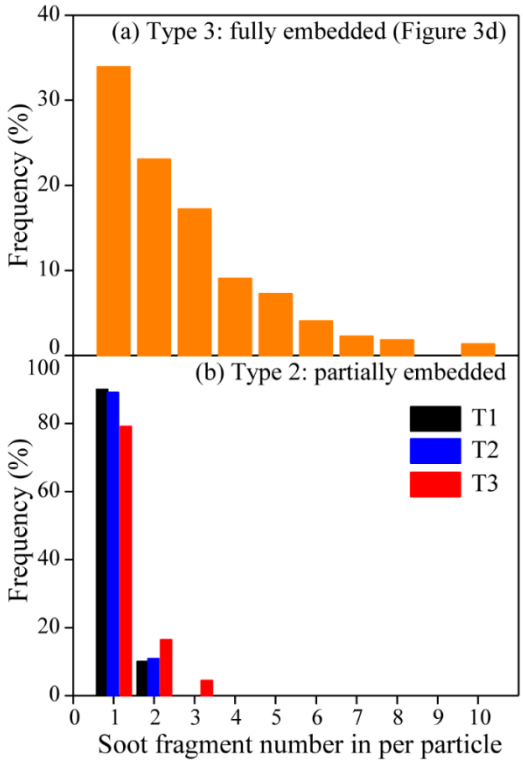

Figure S7. Frequency of soot fragment number in single soot-bearing particles.

6. Need to discuss how many soot particles were studied per sample. How many total samples during event? Overall, particle statistic is poor.

Answer: Totally, we analyzed seven dust samples (Table S1). The number of analyzed soot-bearing particles is shown above the column in Figure 4. The total number of aerosol particles analyzed in this study is presented in the 2.2, which is 412, 486, and 887 for T1, T2, and T3 site, respectively.

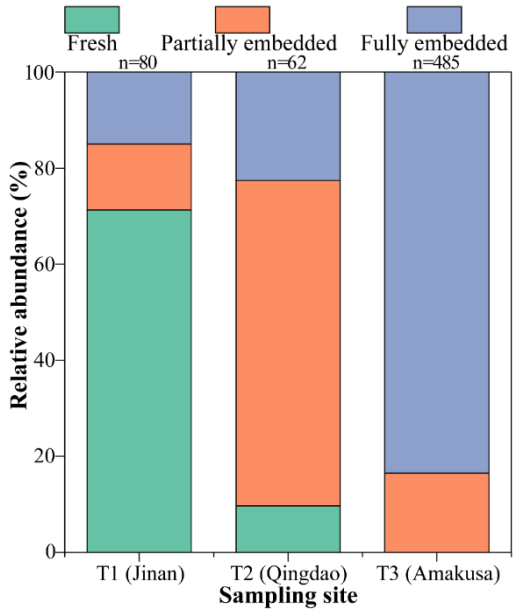

Figure 4. Relative abundance of three types of soot-bearing aerosol particles at the three sampling sites. The number of analyzed soot-bearing particles is shown above the column.

7. If phase separation may be a key mechanism for observation of fully embedded particles, the authors can investigate fraction of fully embedded particles at different RH, not just by sampling site. The RH was high too during certain time at T2 site. The authors should investigate those samples as well.

Answer: There might be some misunderstanding. We did not propose that phase separation may be a key mechanism for fully embedded particles. The high RH in marine air could lead to secondary aerosols change from a solid to liquid phase. During or after sampling, due to the RH decreasing, the phase separation between inorganic and organic components occur. This is a possible cause of the formation of scattered tiny soot in the organic coating (special mixing structure in Figure 3d).

References

Li, W., Sun, J., Xu, L., Shi, Z., Riemer, N., Sun, Y., Fu, P., Zhang, J., Lin, Y., Wang, X., Shao, L., Chen, J., Zhang, X., Wang, Z., and Wang, W.: A conceptual framework for mixing structures in individual aerosol particles, J. Geophys. Res.: Atmos., 121, 13784-13798, https://doi.org/10.1002/2016JD025252, 2016.

Li, W. J., and Shao, L. Y.: Observation of nitrate coatings on atmospheric mineral dust particles, Atmos. Chem. Phys., 9, 1863-1871, https://doi.org/10.5194/acp-9-1863-2009, 2009.

Tracing the evolution of morphology and mixing state of soot particles along with the movement of an Asian dust storm

Liang Xu[1], Satoshi Fukushima[2], Sophie Sobanska[3], Kotaro Murata[2], Ayumi Naganuma[2], Lei Liu[1], Yuanyuan Wang[1], Hongya Niu[4], Zongbo Shi[5], Tomoko Kojima[6], Daizhou Zhang[2], Weijun Li[1,*]

[1]Department of Atmospheric Sciences, School of Earth Sciences, Zhejiang University, Hangzhou 310027, China

[2]Faculty of Environmental and Symbiotic Sciences, Prefectural University of Kumamoto, Kumamoto 862-8502, Japan

[3]Institute of Molecular Sciences, UMR CNRS 5255, University of Bordeaux, 351 cours de la libération, 33405 Talence, France

[4]Key Laboratory of Resource Exploration Research of Hebei Province, Hebei University of Engineering, Handan 056038, Hebei, China

[5]School of Geography, Earth and Environmental Sciences, University of Birmingham, UK

[6]Department Earth and Environmental Science, Faculty of Advanced Science and Technology, Kumamoto University, Kumamoto 860-8555, Japan

*Corresponding author: W. Li (liweijun@zju.edu.cn)

Department of Atmospheric Sciences, School of Earth Sciences, Zhejiang University, Hangzhou 310027, China

Abstract

Tracing the aging progress of soot particles during transport is highly challenging. An Asian dust event could provide an ideal opportunity to trace the continuous aging progress of long-range transported soot particles. Here, we collected individual aerosol particles at an inland urban site (T1) and a coastal urban site (T2) in China and a coastal site (T3) in southwestern Japan during an Asian dust event. Microscopic analysis showed that the number fraction of soot-bearing particles was 19% and 16% at T1 and T2 in China but surprisingly increased to 56% at T3 in Japan. The dominant fresh soot (71%) at T1 became partially embedded (68%) at T2 and fully embedded (84%) at T3. These results indicated that the tiny soot particles had lower deposition than other aerosol types and became more aged during the transport from T1 to T3. We quantified soot morphology using the fractal dimension and found the trend from 1.65 at T1, 1.84 at T2, and to 1.91 at T3. Furthermore, we found that the morphology compression of the soot aggregations was associated with secondary coating thickness and relative humidity. A unique mixing structure that multi-soot particles scattered in organic coatings instead of sulfate core in individual core-shell particles was observed at T3 after the crossing of the East China Sea. The study well understands important constraints of the soot morphological effects and provides possible aging scale along with their transport pathway. These new findings will be helpful to improve optical calculation and regional climate modeling of soot particles during their transport in the atmosphere.

1. Introduction

Soot (i.e., black carbon (BC)) is a type of carbonaceous material with graphitic structures emitted from the incomplete combustion of fossil fuels and biomass. Soot particles exhibit a chain-like aggregation morphology with a diameter of 10 nm to 100 nm (Buseck et al., 2014). Because of its strong capacity to absorb solar radiation, soot is considered the second greatest contributor to global warming after carbon dioxide (IPCC., 2013;Bond et al., 2013). Soot is an important particulate pollutant in fine particles (i.e., $PM_{2.5}$) in urban polluted air, which adversely affects the respiratory health of citizens and induces generally unwanted heating in the planetary boundary layer (West et al., 2016;Ding et al., 2016).

Fresh soot particles are hydrophobic but are converted into a hydrophilic state following their aging through physical and chemical processes (Li et al., 2016b;Riemer et al., 2010;Perring et al., 2017). Aged soot particles containing secondary coating aerosols (e.g., ammonium sulfate, ammonium nitrate, and organic matter) can be activated as cloud condensation nuclei (CCN) (Zhang et al., 2008;Wang et al., 2010;Ding et al., 2019;Shiraiwa et al., 2007;Lee et al., 2019). These coatings can significantly change the optical scattering and absorption capacity of soot particles (Liu et al., 2017;Moffet and Prather, 2009;Matsui et al., 2018;He et al., 2015;Zhang et al., 2018a). Numerical model simulations have estimated that light absorption by internally mixed soot is enhanced by a factor of 2 over externally mixed soot (Jacobson, 2001). In contrast, Cappa et al. (2012) reported in situ observations of soot absorption enhancement of only 6% in ambient air. This discrepancy between simulation and

observation could be attributed to the complex mixing structure and various morphologies of soot particles in the air (Adachi et al., 2016;Li et al., 2016a;Wu et al., 2018).

In aged air masses, soot particles tend to be internally mixed with secondary aerosols such as sulfates, nitrates, and secondary organic matter (Li et al., 2016b). Especially in the East Asian region, one of the most polluted areas in the world, soot is internally mixed with secondary aerosols in polluted urban, rural, and remote air (Adachi et al., 2016;Zhang et al., 2013;Yuan et al., 2019;Zhang et al., 2018b). However, most of these studies have focused on the aging and mixing state of soot particles at one or multiple isolated sites. These results have not traced the detailed aging processes (e.g., morphology and mixing structure) from fresh to aged soot particles during their transport.

Although great progress has been made in the field of soot aging, it is highly challenging to trace the aging processes of soot particles during transport. Asian dust storms carry both dust and anthropogenic aerosols across East Asia into the North Pacific Ocean (Li et al., 2014;Geng et al., 2014;Zhang et al., 2005). This presents an ideal environment to study the aging processes of soot particles during long-range transport. Compared to previous publications, the present study quantified the variation in mixing structures and fractal dimension of soot particles and further explored how shape of soot particles changed following the dust storm movement from East China to Japan.

Using transmission electron microscopy (TEM), we investigated the morphology,

mixing structure, relative abundance, and size distribution of individual soot particles. Furthermore, we evaluated the morphological differences of individual soot particles at three sampling sites. Finally, a conceptual model was proposed to better understand the aging processes of long-rang transported soot particles.

2. Experimental methods

2.1 Aerosol sampling

Three sampling sites were chosen for aerosol collections: an inland urban site in Jinan city (T1, 36.67°N 117.06°E), China, a coastal urban site in Qingdao city (T2, 36.10°N 120.46°E), China, and a coastal rural site at Amakusa (T3, 32.30°N 130.00°E) in southwestern Japan (Figure 1). A dust storm outbreak was observed in East Asia. Detailed information about this dust storm will be discussed in Section 3.1. We collected aerosol particles during dust transport from 18 to 19 March 2014 at the three sampling sites (Figure S1-S5). In total, seven dust samples were collected within 30 hours after the dust storm arrival. The details about the sampling dates, times, meteorological conditions, and PM (particulate matter) concentrations for the samples are listed in Table S1.

A DKL-2 sampler (Genstar Electronic Technology, China) was used to collect individual aerosol particles on copper TEM grids covered by carbon film (carbon type-B, 300-mesh copper; Tianld Co., China) with an air flow of 1.0 L/min. A single-stage impactor with a 0.5 mm diameter jet nozzle was installed on the sampler. This impactor has a collection efficiency of 100% at an aerodynamic diameter of 0.5 μm with an assumed particle density of 2 g/cm^3. The sampling duration varied from 1 min to 2 min

according to the visibility, PM concentration, and particle distribution on the substrate. All samples were placed in sealed, dry plastic capsules and stored in a desiccator at 25 °C and 20 ± 3% relative humidity (RH) for further analysis.

2.2 Electron microscopic analyses

A JEOL JEM-2100 transmission electron microscopy (TEM) operated at 200 kV was used to analyze individual particles. Elemental composition was determined semiquantitatively by using an energy-dispersive X-ray spectrometer (EDS) (Oxford Instruments, UK) that can detect elements heavier than carbon ($Z \geq 6$). The distribution of aerosol particles on TEM grids was not uniform, with coarser particles occurring near the center and finer particles occurring on the periphery (Xu et al., 2019). Therefore, to ensure that the analyzed particles were representative of the entire size range, three areas were chosen from the center to the periphery of the sampling spot on each grid. iTEM software (Olympus Soft Imaging Solutions GmbH, Germany) was used to analyze the TEM images and obtain the projected area, perimeter, shape factor, and equivalent circle diameter (ECD) of individual aerosol particles. In total, we analyzed 412, 486, and 887 aerosol particles for T1, T2, and T3 site, respectively.

2.3 AFM analysis

Atomic force microscopy (AFM) is an analytical method used for studying the surface structure of solid materials. AFM (Dimension Icon, Germany) can determine the three-dimensional morphology of particles in tapping mode. The AFM settings consisted of imaging forces between 1 and 1.5 nN, scanning rates between 0.5 and 0.8 Hz, and a scanning range of 10 μm with a resolution of 512 pixels per length. The

bearing areas (A) and bearing volumes (V) of the particles were directly obtained from NanoScope Analysis software. Their equivalent circle diameters (ECDs) and equivalent volume diameters (EVDs) were calculated according to the formulas described by Chi et al. (2015).

The correlations of ECDs and EVDs are shown in Figure S6 in the Supporting Information. Therefore, the ECD of individual aerosol particles measured from the iTEM software can be further converted into an EVD based on this correlation.

2.4 Air mass backward trajectories

Forty-eight hour backward trajectories were calculated for the three sites using the NOAA HYSPLIT (Hybrid Single Particle Lagrangian Integrated Trajectory) trajectory model (Stein et al., 2015). We selected an altitude of 1500 m as the end point in each backward trajectory.

We measured the actual duration from the Beijing-Tianjin-Hebei (BTH) area to T1 and T2 according to the backward trajectories in Figure 1. It was approximately 12 hours between BTH and T1 and 15 hours between BTH and T2. The interval between T1 and T2 was three hours. The duration between the air mass leaving T2 and reaching T3 was approximately 30 hours.

2.5 Morphological analysis of soot particles

The fractal dimension (D_f) calculated by the scaling law is used to characterize the morphology of soot particles (Koeylue et al., 1995).

$$N=k_g\left(\frac{2R_g}{d_p}\right)^{D_f} \quad (1)$$

where N is the total number of soot monomers, R_g is the radius of gyration of the soot

155 particle, d_p is the diameter of soot monomer, k_g is the fractal prefactor, and D_f is the
156 mass fractal dimension of an individual soot particle.

157 D_f and k_g in Equation 1 are estimated from a power law fit of a scatter plot of N
158 versus the values of $2R_g/d_p$. N can also be calculated by Equation 2.

159 $$N=k_a\left(\frac{A_a}{A_p}\right)^{\alpha} \quad (2)$$

160 where A_a is the projected area of the soot particle, A_p is the mean projected area of the
161 soot monomer, k_a is a constant, and α is an empirical projected area exponent.

162 The values of α and k_a in Equation 2 depend on the overlap parameter (δ) calculated
163 using Equation 3. Then δ can be used to obtain α and k_a based on Fig. 6. in Oh and
164 Sorensen (1997).

165 $$\delta=\frac{2a}{l} \quad (3)$$

166 where a is the soot monomer radius and l is the monomer spacing.

167 The radius of gyration of the soot particle R_g is obtained by the simple
168 correlation in Equation 4 developed by Brasil et al. (1999)

169 $$L_{max}/(2R_g)=1.50 \pm 0.05 \quad (4)$$

170 where L_{max} is the maximum length of the soot particle.

171 The values of d_p, A_a, A_p, a, l, and L_{max} can be directly obtained from TEM images.

172 In addition to D_f, we also used the shape factor (SF) to further quantify the
173 morphological differences of soot particles. The shape factor is defined as the ratio of
174 the actual area of a particle to the area of a circle with the same perimeter (Equation 5).
175 A shape factor of 1 (the maximum value) indicates a perfectly round particle.

176 $$SF=\frac{4\pi S}{P^2} \quad (5)$$

where S is the area of a soot particle and P is the perimeter of a soot particle.

3. Results and discussion

3.1 The Asian dust storm event

Figure 2 displays variations in PM_{10} and $PM_{2.5}$ concentrations before, during, and after the dust storm event at the Jinan, Qingdao, and Amakusa sampling sites. The dust storm air mass started to influence T1 at approximately 06:00 on 03/17 (Universal Time Coordinated, UTC). The concentration of PM_{10} at T1 increased rapidly to a maximum value of 834 μg/m^3. The air mass reached T2 at 09:00 on 03/17, and the highest PM_{10} concentration was recorded at 721 μg/m^3. After the arrival of a cold front at T2, the air mass continued moving approximately 1000 km to T3 at 02:00 on 03/18. The concentration of PM_{10} reached 87 μg/m^3 at T3 (Figure 2). During this study, the meteorological data (e.g., temperature and air pressure) measured at the three sampling sites also confirm the arrival time of the dust storm (Figures S3-S5). All seven dust samples were collected after the arrival of the dust storm, thus confirming the sampling of the same dust storm event (Figures 2 and S2).

Figure 1 indicates that all the air masses during the dust storm event originated from Mongolia, moving southeastward via the BTH area, reaching T1 and T2. The BTH, as the largest city cluster in China, contains one of the largest anthropogenic emission sources (e.g., heavy industries, coal-fired power plants, and vehicles) in the world (Li et al., 2016b). The transport duration from the BTH to T1 and T2 was about 12 hours and 15 hours, respectively. Thus, we estimated that the interval between T1 and T2 was three hours. After passing over T1 and T2, the air masses kept moving southeastward to Japan. The estimated interval between T2 and T3 was 30 hours. The ground PM and meteorological measurements at the three sampling sites (Figure 2 and S3-S5) coupled

with air mass back trajectories (Figure 1) and a dust storm simulation in East Asia (Figure S1) together verified that the dust storm event, under the force of a strong cold front, transported across the large BTH city cluster to the downwind area. Therefore, this dust storm movement provides a unique opportunity to study particles in the same air mass and thus trace physical and chemical changes in aerosol particles.

3.2 Classification and mixing state of soot-bearing particles

Soot particles with a typical chain-like structure can be easily distinguished from other aerosol components (e.g., sulfate, organic, metal, and mineral particles) by their morphology. TEM observation is a convenient way to determine whether soot is associated with other aerosol components (Li et al., 2016b;Laskin et al., 2019). During the dust storm period, 56% of the analyzed particles within a size range of 50 nm to 2.4 μm included soot particles at T3, approximately three times higher than those at T1 (19%) and T2 (16%). This high percentage of internally mixed soot particles was also shown by Ueda et al. (2016) in an Asian outflow at Noto Peninsula, Japan, based on single-particle soot photometer (SP2) analyses. Our results show that the dust storm event not only carried large amounts of dust particles from the Gobi Desert in northwestern China but that this dust-laden air mass also incorporated many soot particles from polluted East Asia (Figure 2 and Figure 3a-d). This is consistent with Pan et al. (2015), who showed that dust storms in East Asia contain and transport anthropogenic pollutants from urban areas.

Based on the mixing structures between soot and sulfate on the substrates, three groups of soot particles were defined in this study: fresh, partially embedded and fully embedded (Figure 3).

Fresh soot. The soot particles were not obviously mixed with secondary aerosol

components (Figure 3a). Although surfaces of the fresh soot particles could contain minor organic matter, the organic film was insufficient to change soot morphology and optical properties (Buseck et al., 2014).

Partially embedded soot. Part of the soot particle was coated by secondary aerosols (Figure 3b). Most of partially embedded soot particles include one soot core, only ~ 10% of them contain two soot cores (Figure S7).

Fully embedded soot. The entire soot particle was encapsulated by secondary aerosols (Figure 3c). It should be noted that some soot particles were only embedded in the organic coating instead of the sulfur-rich core (Figure 3d).

TEM images show that the fully embedded soot particles with a clear rim on the substrate displayed a droplet-like shape (Figure 3c-d), suggesting that these secondary particles were in an aqueous phase in ambient air (Li et al., 2016b).

Based on the three mixing structures of soot particles, we further obtained their relative abundance at the three sampling sites (Figure 4). Seventy-one percent of soot-bearing particles were fresh at T1, decreasing to 10% at T2. In contrast, partially embedded soot increased from 14% at T1 to 68% at T2 when the cold front moved from T1 to T2. It should be noted that fresh soot disappeared at T3 after crossing the East China Sea, and the fully embedded soot dominated soot-bearing particles (84%).

Following the dust storm movement, we found that the number fraction of total soot-bearing particles increased to 56% among all the analyzed particles from T1 to T3, suggesting that soot particles had lower deposition than other aerosol types in the cold front. Indeed, soot particles normally have smaller sizes and densities than mineral dust,

metal, sulfate, and nitrate particles (Peng et al., 2017), suggesting that soot particles can be transported over longer distances during Asian dust storms. Moreover, the number fraction increase of soot-bearing particles also could be attributed to the increase of mixing state index (the metric to quantify the population mixing state, ranging from 0 for a completely external mixture to 1 for a completely internal mixture) as aging during transport (Riemer and West, 2013;Healy et al., 2014).

3.3 Quantifying the morphology of soot particles

The fractal dimension (D_f) of soot particles is a key parameter used to reflect soot morphological structure; e.g., compact soot particles usually have larger D_f than lacy aggregates (China et al., 2015;Wang et al., 2017;China et al., 2013). Therefore, D_f can be used to understand soot aging processes in the atmosphere. Figure 5 shows that the D_f sequence of soot particles is T1 (1.65) < T2 (1.84) < T3 (1.91). The D_f of soot particles at T1 (1.65) is much closer to the values of soot emitted from sources, such as the D_f from biomass burning in the range of 1.68−1.74 (Chakrabarty et al., 2006) and the D_f from diesel burning in the range of 1.56−1.68 (Wentzel et al., 2003). The D_f of soot particles at T3 (1.96 for partially embedded soot and 1.88 for fully embedded soot, Figure S8) is close to that of aged soot (1.81-1.90) in remote marine air (China et al., 2015) and polluted air in North China (Wang et al., 2017).

At the three sampling sites, the highest D_f value at T3 suggests a more compacted structure of the soot particles. Moreover, we obtained the shape factors of soot particles at the three sampling sites to indicate the compactness of soot particle. The average shape factor of soot particles at T3 was 0.73, much higher than 0.34 at T1 and 0.54 at

T2 (Figure 6a). These two parameters show that the soot morphology became more compact and had a rounder shape following the dust storm movement.

3.4 Soot-bearing particle size growth following soot aging

The average ratio (D_p/D_{core}) of the diameter of the internally mixed particle (D_p) to its corresponding soot core (D_{core}) during the dust storm period was 1.42 at T1, 1.78 at T2, and 2.49 at T3 (Figure 6b). Size distribution of the soot core indicates a small difference between T1, T2, and T3 during the dust storm period (peak at 200-250 nm, Figure S9). Thus, the D_p/D_{core} increase from T1 to T3 is attributed to the increased coating thickness. The D_p/D_{core} values in this study are much higher than the reported values in fresh emissions (e.g., average value 1.24 for fossil fuel (Sahu et al., 2012)) but close to ~2.0 in aged aerosols in background and polluted air (Dahlkötter et al., 2014;Raatikainen et al., 2015;Metcalf et al., 2012). Recently, Peng et al. (2017) reported a high growth rate in urban Beijing and a derived average D_p/D_{core} value of 1.97 (1.34-2.61). The D_p/D_{core} value in urban Beijing air is much higher than our reported values of 1.42-1.78 at T1 and T2 during the dust storm period. This is understandable considering the weak secondary aerosol formation in the dust storm in the continental air as a result of acidic gases being scavenged by the large amounts of mineral dust particles (Li et al., 2016b).

Based on the air mass backward trajectories, we can infer that it took approximately three hours for the cold front to move between T1 and T2 and 30 hours from T2 to T3 (Figure 1). Here, we calculated the coating volume of aged soot particles based on the values of D_p and D_{core} of individual particles and found a 152% increase in the coating volume from T1 to T2 and a 609% increase from T2 to T3.

3.5 Aging mechanism of soot particles

We noticed that the partially embedded soot particles significantly increased from

14% at T1 to 68% at T2 (Figure 4), indicating that the fresh soot particles aged during the dust storm movement from the inland to the coastal area. Meanwhile, we found that the D_f value at T1 changed from 1.65 at T1 to 1.84 at T2. The strong diffusion during the dust storm is not conducive to soot accumulation (Pan et al., 2015). Although local emissions at T2 could interference the observation of soot aging process, long-range transported soot particles were still dominant at T2 during the cold front. These results indicate that the morphological structures of soot particles underwent changes along with the dust storm movement. In a word, large amounts of fresh soot converted into partially embedded soot particles from T1 to T2 (Figure 4).

Figure 4 shows that the fresh soot particles disappeared at T3, and the number fraction of fully embedded soot particles increased to 84%. Moreover, the D_f of soot particles had a large change from 1.84 at T2 to 1.91 at T3, which suggests that the morphology structure of soot particles changed from chain-like to compact when the air masses crossed the East China Sea (Figure 5).

Secondary aerosol formation on soot particles can significantly change their fractal morphology into a compact shape (China et al., 2015;Wang et al., 2017;Ma et al., 2013;Pei et al., 2018). The thick coating of soot particles occurred when air masses crossed the East China Sea (Figure 6b), suggesting that secondary aerosol coating formation can significantly compress the fractal morphology of soot particles. Recently, Yuan et al. (2019) further found that the phase change of secondary aerosols (due to RH variation) in aged soot particles could further compress the fractal shape of soot aggregates. The high humidity in marine air (T2 to T3) should lead to phase changes of secondary aerosols and further cause the morphological compactness of soot aggregations. These two reasons are able to explain the change in soot fractal dimension from T2 to T3 (Figure 5).

TEM observations present a particular mixing structure of the fully embedded soot at T3: organic coating instead of sulfate contains several typical soot particles, and the organic coating spreads on the substrate (named droplet-like particles (O'Brien et al., 2015;Li et al., 2011)) (Figures 3d and 7c). More than half of this type of particles contain one or two soot fragments, while 43% of them include more than three soot fragments (Figure S7). The droplet-like coating morphology of soot can reflect that these secondary particles were in an aqueous phase at T3 in the air. Similar droplet-like particles were not observed at T1 and T2 (Figure 7a and b). A previous study has shown that secondary aerosol particles begin to acquire aqueous shells at RH 60% (Sun et al., 2018). Once secondary aerosols change from a solid to liquid phase following an RH increase in marine air, soot particles tend to adhere to the liquid phase through coagulation (Li et al., 2016b). Figure 7c shows the phase separation of the organic coating and sulfate core on the substrate under the phenomenon of liquid-liquid phase separations (You et al., 2012). Recently, Brunamonti et al. (2015) found that soot particles tend to redistribute into the organic coating during liquid-liquid phase separation. Therefore, the soot distribution in the organic coating indicates that aerosol particles in the air mass at T3 underwent an aqueous aging process over the East China Sea, which is different from the continental aerosol particles at T1 and T2. It must be noted that several tiny soot particles were distributed in the organic coating at T3 (Figure 7c), which did not occur at T1 and T2. There is no previous study to report the tiny scattered soot in the organic coating. We proposed a possible reason that soot particle with smaller size have a longer lifetime and could be transported over longer distances. Therefore, the tiny soot particles have more chances to coagulate with preexisting aqueous secondary particles in marine air (Liu et al., 2018). Our findings suggest that the complex aqueous process of individual particles in marine air could

result in scattered soot particles, but further studies are required to reveal the detailed reasons.

Tracing the soot particles during the dust storm, we can clarify that the morphology change of soot particles depends on the secondary coating thickness and relative humidity in the air. The microscopic changes between soot and coating could change their optical absorption, which is different from the core-shell absorption (He et al., 2015). Our study proposes that BC-related optical models should not only consider the mixing state of soot particles but also incorporate the morphological structure of soot particles in different environmental air.

Based on the results and discussion above, we propose a conceptual model to summarize the evolution of morphology and mixing state of soot particles along with the movement of an Asian dust storm (Figure 8). Dust storms in East Asia could carry soot and other anthropogenic pollutants from urban areas to downwind areas. During the transport, the dominated mixing structure of individual soot particles changed from fresh to partially embedded and finally to fully embedded. Meanwhile, the chain-like soot compressed and had a rounder shape depending on secondary coating thickness and relative humidity.

4. Conclusions

Individual aerosol particles were collected from 18 to 19 March 2014 during an Asian dust storm event. Three sampling sites along with the pathway of the dust storm were chosen to study soot aging, including an inland urban site in Jinan city, China (T1), a coastal urban site in Qingdao city, China (T2), and a coastal rural site at Amakusa in southwestern Japan (T3). Soot-bearing particles were classified into three types: fresh, partially embedded, and fully embedded. There was a noticeable difference in the

mixing structure of soot particles during long-range transport, with 71% fresh soot in the analyzed soot particles (by number) at T1, 68% partially embedded soot at T2, and 84% fully embedded soot at T3. The fractal dimension (D_f) of soot particles at T3 (1.91) was higher than that at the other two sites (1.65 and 1.84), suggesting that soot particles converted from chain-like to compact shapes during long-range transport. This study showed that an increasing number of soot particles were internally mixed with secondary aerosol particles and significantly aged during transport. The average ratio of D_p/D_{core} during the dust storm period was 1.42 at T1, 1.78 at T2, and 2.49 at T3, indicating increasing coating thickness. By comparing the soot fractal dimension in continental air and marine air, we found that secondary coating thickness and relative humidity both can significantly change the fractal morphology of soot particles in the air. Individual particle analysis showed that several tiny soot particles only observed in organic coatings instead of sulfate in individual soot-bearing particles at T3.

Data availability

All data presented in this paper are available upon request from the corresponding author (liweijun@zju.edu.cn).

Supporting information

Table S1 and Figures S1-S9

Author contributions

LX and WL conceived the study and wrote the manuscript. The field campaign was organized and supervised by WL and DZ. SF, KM, AN, and TK collected aerosol

particles. LX, SS, LL, YW, HN, and ZS contributed sample and data analyses. All authors reviewed and commented on the paper.

Competing interests

The authors declare that they have no conflict of interest.

Acknowledgments

We thank Peter Hyde for his editorial comments. This work was funded by the National Natural Science Foundation of China (42075096, 91844301, 41807305), the National Key R&D Program of China (2017YFC0212700), Zhejiang Provincial Natural Science Foundation of China (LZ19D050001), and China Postdoctoral Science Foundation (2019M662021).

References

Adachi, K., Moteki, N., Kondo, Y., and Igarashi, Y.: Mixing states of light-absorbing particles measured using a transmission electron microscope and a single-particle soot photometer in Tokyo, Japan, J. Geophys. Res.: Atmos., 121, 9153-9164, https://doi.org/10.1002/2016JD025153, 2016.

Bond, T. C., Doherty, S. J., Fahey, D. W., Forster, P. M., Berntsen, T., DeAngelo, B. J., Flanner, M. G., Ghan, S., Kärcher, B., Koch, D., Kinne, S., Kondo, Y., Quinn, P. K., Sarofim, M. C., Schultz, M. G., Schulz, M., Venkataraman, C., Zhang, H., Zhang, S., Bellouin, N., Guttikunda, S. K., Hopke, P. K., Jacobson, M. Z., Kaiser, J. W., Klimont, Z., Lohmann, U., Schwarz, J. P., Shindell, D., Storelvmo, T., Warren, S. G., and Zender, C. S.: Bounding the role of black carbon in the climate system: A scientific assessment, J. Geophys. Res.: Atmos., 118, 5380-5552, https://doi.org/10.1002/jgrd.50171, 2013.

Brasil, A. M., Farias, T. L., and Carvalho, M. G.: A recipe for image characterization of fractal-Like aggregates, J. Aerosol Sci, 30, 1379-1389, https://doi.org/10.1016/S0021-8502(99)00026-9, 1999.

Brunamonti, S., Krieger, U. K., Marcolli, C., and Peter, T.: Redistribution of black carbon in aerosol particles undergoing liquid‐liquid phase separation, Geophys. Res. Lett., 42, 2532-2539, https://doi.org/10.1002/2014GL062908, 2015.

Buseck, P. R., Adachi, K., Gelencsér, A., Tompa, É., and Pósfai, M.: Ns-Soot: A Material-Based Term for Strongly Light-Absorbing Carbonaceous Particles, Aerosol Sci. Technol., 48, 777-788, https://doi.org/10.1080/02786826.2014.919374, 2014.

Cappa, C. D., Onasch, T. B., Massoli, P., Worsnop, D. R., Bates, T. S., Cross, E. S., Davidovits, P., Hakala, J., Hayden, K. L., Jobson, B. T., Kolesar, K. R., Lack, D. A., Lerner, B. M., Li, S.-M., Mellon, D., Nuaaman, I., Olfert, J. S., Petäjä, T., Quinn, P. K., Song, C., Subramanian, R., Williams, E. J., and Zaveri, R. A.: Radiative Absorption Enhancements Due to the Mixing State of Atmospheric Black Carbon, Science, 337, 1078-1081, https://doi.org/10.1126/science.1223447, 2012.

Chakrabarty, R. K., Moosmüller, H., Garro, M. A., Arnott, W. P., Walker, J., Susott, R. A., Babbitt, R. E., Wold, C. E., Lincoln, E. N., and Hao, W. M.: Emissions from the laboratory combustion of wildland

fuels: Particle morphology and size, J. Geophys. Res.: Atmos., 111, https://doi.org/10.1029/2005JD006659, 2006.
Chi, J. W., Li, W. J., Zhang, D. Z., Zhang, J. C., Lin, Y. T., Shen, X. J., Sun, J. Y., Chen, J. M., Zhang, X. Y., Zhang, Y. M., and Wang, W. X.: Sea salt aerosols as a reactive surface for inorganic and organic acidic gases in the Arctic troposphere, Atmos. Chem. Phys., 15, 11341-11353, https://doi.org/10.5194/acp-15-11341-2015, 2015.
China, S., Mazzoleni, C., Gorkowski, K., Aiken, A. C., and Dubey, M. K.: Morphology and mixing state of individual freshly emitted wildfire carbonaceous particles, Nat. Commun., 4, 2122, https://doi.org/10.1038/ncomms3122, 2013.
China, S., Scarnato, B., Owen, R. C., Zhang, B., Ampadu, M. T., Kumar, S., Dzepina, K., Dziobak, M. P., Fialho, P., and Perlinger, J. A.: Morphology and mixing state of aged soot particles at a remote marine free troposphere site: Implications for optical properties, Geophys. Res. Lett., 42, 1243-1250, https://doi.org/10.1002/2014GL062404, 2015.
Dahlkötter, F., Gysel, M., Sauer, D., Minikin, A., Baumann, R., Seifert, P., Ansmann, A., Fromm, M., Voigt, C., and Weinzierl, B.: The Pagami Creek smoke plume after long-range transport to the upper troposphere over Europe – aerosol properties and black carbon mixing state, Atmos. Chem. Phys., 14, 6111-6137, https://doi.org/10.5194/acp-14-6111-2014, 2014.
Ding, A. J., Huang, X., Nie, W., Sun, J. N., Kerminen, V. M., Petäjä, T., Su, H., Cheng, Y. F., Yang, X. Q., Wang, M. H., Chi, X. G., Wang, J. P., Virkkula, A., Guo, W. D., Yuan, J., Wang, S. Y., Zhang, R. J., Wu, Y. F., Song, Y., Zhu, T., Zilitinkevich, S., Kulmala, M., and Fu, C. B.: Enhanced haze pollution by black carbon in megacities in China, Geophys. Res. Lett., 43, 2873-2879, https://doi.org/10.1002/2016GL067745, 2016.
Ding, S., Liu, D., Zhao, D., Hu, K., Tian, P., Zhou, W., Huang, M., Yang, Y., Wang, F., Sheng, J., Liu, Q., Kong, S., Cui, P., Huang, Y., He, H., Coe, H., and Ding, D.: Size-Related Physical Properties of Black Carbon in the Lower Atmosphere over Beijing and Europe, Environ. Sci. Technol., 53, 11112-11121, https://doi.org/10.1021/acs.est.9b03722, 2019.
Geng, H., Hwang, H., Liu, X., Dong, S., and Ro, C. U.: Investigation of aged aerosols in size-resolved Asian dust storm particles transported from Beijing, China, to Incheon, Korea, using low-Z particle EPMA, Atmos. Chem. Phys., 14, 3307-3323, https://doi.org/10.5194/acp-14-3307-2014, 2014.
He, C., Liou, K. N., Takano, Y., Zhang, R., Levy Zamora, M., Yang, P., Li, Q., and Leung, L. R.: Variation of the radiative properties during black carbon aging: theoretical and experimental intercomparison, Atmos. Chem. Phys., 15, 11967-11980, https://doi.org/10.5194/acp-15-11967-2015, 2015.
Healy, R. M., Riemer, N., Wenger, J. C., Murphy, M., West, M., Poulain, L., Wiedensohler, A., O'Connor, I. P., McGillicuddy, E., Sodeau, J. R., and Evans, G. J.: Single particle diversity and mixing state measurements, Atmos. Chem. Phys., 14, 6289-6299, https://doi.org/10.5194/acp-14-6289-2014, 2014.
IPCC.: Clouds and Aerosols. In: Climate Change 2013: The Physical Science Basis, Contribution of Working Group I to the Fifth Assessment Report of the Intergovernmental Panel on Climate Change. Intergovernmental Panel on Climate Change (IPCC), 571- 657, 2013.
Jacobson, M. Z.: Strong radiative heating due to the mixing state of black carbon in atmospheric aerosols, Nature, 409, 695-697, https://doi.org/10.1038/35055518, 2001.
Koeylue, U., Xing, Y., and Rosner, D. E.: Fractal Morphology Analysis of Combustion-Generated Aggregates Using Angular Light Scattering and Electron Microscope Images, Langmuir, 11, 4848-4854, https://doi.org/10.1021/la00012a043, 1995.
Laskin, A., Moffet, R. C., and Gilles, M. K.: Chemical Imaging of Atmospheric Particles, Acc. Chem.

Res., 52, 3419-3431, https://doi.org/10.1021/acs.accounts.9b00396, 2019.
Lee, A. K. Y., Rivellini, L.-H., Chen, C.-L., Liu, J., Price, D. J., Betha, R., Russell, L. M., Zhang, X., and Cappa, C. D.: Influences of Primary Emission and Secondary Coating Formation on the Particle Diversity and Mixing State of Black Carbon Particles, Environ. Sci. Technol., 53, 9429-9438, https://doi.org/10.1021/acs.est.9b03064, 2019.
Li, J., Liu, C., Yin, Y., and Kumar, K. R.: Numerical investigation on the Ångström exponent of black carbon aerosol, J. Geophys. Res.: Atmos., 121, 3506-3518, https://doi.org/10.1002/2015JD024718, 2016a.
Li, W., Zhou, S., Wang, X., Xu, Z., Yuan, C., Yu, Y., Zhang, Q., and Wang, W.: Integrated evaluation of aerosols from regional brown hazes over northern China in winter: Concentrations, sources, transformation, and mixing states, J. Geophys. Res.: Atmos., 116, D09301, https://doi.org/10.1029/2010JD015099, 2011.
Li, W., Shao, L., Shi, Z., Chen, J., Yang, L., Yuan, Q., Yan, C., Zhang, X., Wang, Y., Sun, J., Zhang, Y., Shen, X., Wang, Z., and Wang, W.: Mixing state and hygroscopicity of dust and haze particles before leaving Asian continent, J. Geophys. Res.: Atmos., 119, 1044-1059, https://doi.org/10.1002/2013JD021003, 2014.
Li, W., Sun, J., Xu, L., Shi, Z., Riemer, N., Sun, Y., Fu, P., Zhang, J., Lin, Y., Wang, X., Shao, L., Chen, J., Zhang, X., Wang, Z., and Wang, W.: A conceptual framework for mixing structures in individual aerosol particles, J. Geophys. Res.: Atmos., 121, 13784-13798, https://doi.org/10.1002/2016JD025252, 2016b.
Liu, D., Whitehead, J., Alfarra, M. R., Reyes-Villegas, E., Spracklen, D. V., Reddington, C. L., Kong, S., Williams, P. I., Ting, Y.-C., Haslett, S., Taylor, J. W., Flynn, M. J., Morgan, W. T., McFiggans, G., Coe, H., and Allan, J. D.: Black-carbon absorption enhancement in the atmosphere determined by particle mixing state, Nat. Geosci., 10, 184-188, https://doi.org/10.1038/ngeo2901, 2017.
Liu, L., Zhang, J., Xu, L., Yuan, Q., Huang, D., Chen, J., Shi, Z., Sun, Y., Fu, P., Wang, Z., Zhang, D., and Li, W.: Cloud scavenging of anthropogenic refractory particles at a mountain site in North China, Atmos. Chem. Phys., 18, 14681-14693, https://doi.org/10.5194/acp-18-14681-2018, 2018.
Ma, X., Zangmeister, C. D., Gigault, J., Mulholland, G. W., and Zachariah, M. R.: Soot aggregate restructuring during water processing, J. Aerosol Sci, 66, 209-219, https://doi.org/10.1016/j.jaerosci.2013.08.001, 2013.
Matsui, H., Hamilton, D. S., and Mahowald, N. M.: Black carbon radiative effects highly sensitive to emitted particle size when resolving mixing-state diversity, Nat. Commun., 9, 3446, https://doi.org/10.1038/s41467-018-05635-1, 2018.
Metcalf, A. R., Craven, J. S., Ensberg, J. J., Brioude, J., Angevine, W., Sorooshian, A., Duong, H. T., Jonsson, H. H., Flagan, R. C., and Seinfeld, J. H.: Black carbon aerosol over the Los Angeles Basin during CalNex, J. Geophys. Res.: Atmos., 117, D00V13, https://doi.org/10.1029/2011JD017255, 2012.
Moffet, R. C., and Prather, K. A.: In-situ measurements of the mixing state and optical properties of soot with implications for radiative forcing estimates, Proc. Natl. Acad. Sci. U.S.A., 106, 11872-11877, https://doi.org/10.1073/pnas.0900040106, 2009.
O'Brien, R. E., Wang, B., Kelly, S. T., Lundt, N., You, Y., Bertram, A. K., Leone, S. R., Laskin, A., and Gilles, M. K.: Liquid–Liquid Phase Separation in Aerosol Particles: Imaging at the Nanometer Scale, Environ. Sci. Technol., 49, 4995-5002, https://doi.org/10.1021/acs.est.5b00062, 2015.
Oh, C., and Sorensen, C. M.: The Effect of Overlap between Monomers on the Determination of Fractal

513 Cluster Morphology, J. Colloid Interface Sci., 193, 17-25, https://doi.org/10.1006/jcis.1997.5046,
514 1997.
515 Pan, X., Uno, I., Hara, Y., Kuribayashi, M., Kobayashi, H., Sugimoto, N., Yamamoto, S., Shimohara, T.,
516 and Wang, Z.: Observation of the simultaneous transport of Asian mineral dust aerosols with
517 anthropogenic pollutants using a POPC during a long-lasting dust event in late spring 2014, Geophys.
518 Res. Lett., 42, 1593-1598, https://doi.org/10.1002/2014GL062491, 2015.
519 Pei, X., Hallquist, M., Eriksson, A. C., Pagels, J., Donahue, N. M., Mentel, T., Svenningsson, B., Brune,
520 W., and Pathak, R. K.: Morphological transformation of soot: investigation of microphysical
521 processes during the condensation of sulfuric acid and limonene ozonolysis product vapors, Atmos.
522 Chem. Phys., 18, 9845-9860, https://doi.org/10.5194/acp-18-9845-2018, 2018.
523 Peng, J., Hu, M., Guo, S., Du, Z., Shang, D., Zheng, J., Zheng, J., Zeng, L., Shao, M., Wu, Y., Collins,
524 D., and Zhang, R.: Ageing and hygroscopicity variation of black carbon particles in Beijing measured
525 by a quasi-atmospheric aerosol evolution study (QUALITY) chamber, Atmos. Chem. Phys., 17,
526 10333-10348, https://doi.org/10.5194/acp-17-10333-2017, 2017.
527 Perring, A. E., Schwarz, J. P., Markovic, M. Z., Fahey, D. W., Jimenez, J. L., Campuzano-Jost, P., Palm,
528 B. D., Wisthaler, A., Mikoviny, T., Diskin, G., Sachse, G., Ziemba, L., Anderson, B., Shingler, T.,
529 Crosbie, E., Sorooshian, A., Yokelson, R., and Gao, R.-S.: In situ measurements of water uptake by
530 black carbon-containing aerosol in wildfire plumes, J. Geophys. Res.: Atmos., 122, 1086-1097,
531 https://doi.org/10.1002/2016JD025688, 2017.
532 Raatikainen, T., Brus, D., Hyvärinen, A. P., Svensson, J., Asmi, E., and Lihavainen, H.: Black carbon
533 concentrations and mixing state in the Finnish Arctic, Atmos. Chem. Phys., 15, 10057-10070,
534 https://doi.org/10.5194/acp-15-10057-2015, 2015.
535 Riemer, N., West, M., Zaveri, R., and Easter, R.: Estimating black carbon aging time-scales with a
536 particle-resolved aerosol model, J. Aerosol Sci, 41, 143-158,
537 https://doi.org/10.1016/j.jaerosci.2009.08.009, 2010.
538 Riemer, N., and West, M.: Quantifying aerosol mixing state with entropy and diversity measures, Atmos.
539 Chem. Phys., 13, 11423-11439, https://doi.org/10.5194/acp-13-11423-2013, 2013.
540 Sahu, L. K., Kondo, Y., Moteki, N., Takegawa, N., Zhao, Y., Cubison, M. J., Jimenez, J. L., Vay, S.,
541 Diskin, G. S., Wisthaler, A., Mikoviny, T., Huey, L. G., Weinheimer, A. J., and Knapp, D. J.: Emission
542 characteristics of black carbon in anthropogenic and biomass burning plumes over California during
543 ARCTAS-CARB 2008, J. Geophys. Res.: Atmos., 117, D16302,
544 https://doi.org/10.1029/2011JD017401, 2012.
545 Shiraiwa, M., Kondo, Y., Moteki, N., Takegawa, N., Miyazaki, Y., and Blake, D. R.: Evolution of mixing
546 state of black carbon in polluted air from Tokyo, Geophys. Res. Lett., 34, L16803,
547 https://doi.org/10.1029/2007GL029819, 2007.
548 Stein, A. F., Draxler, R. R., Rolph, G. D., Stunder, B. J. B., Cohen, M. D., and Ngan, F.: NOAA's
549 HYSPLIT Atmospheric Transport and Dispersion Modeling System, Bull. Amer. Meteor. Soc., 96,
550 2059-2077, https://doi.org/10.1175/bams-d-14-00110.1, 2015.
551 Sun, J., Liu, L., Xu, L., Wang, Y., Wu, Z., Hu, M., Shi, Z., Li, Y., Zhang, X., Chen, J., and Li, W.: Key
552 Role of Nitrate in Phase Transitions of Urban Particles: Implications of Important Reactive Surfaces
553 for Secondary Aerosol Formation, J. Geophys. Res.: Atmos., 123, 1234-1243,
554 https://doi.org/10.1002/2017JD027264, 2018.
555 Ueda, S., Nakayama, T., Taketani, F., Adachi, K., Matsuki, A., Iwamoto, Y., Sadanaga, Y., and Matsumi,
556 Y.: Light absorption and morphological properties of soot-containing aerosols observed at an East

Asian outflow site, Noto Peninsula, Japan, Atmos. Chem. Phys., 16, 2525-2541, https://doi.org/10.5194/acp-16-2525-2016, 2016.

Wang, J., Cubison, M. J., Aiken, A. C., Jimenez, J. L., and Collins, D. R.: The importance of aerosol mixing state and size-resolved composition on CCN concentration and the variation of the importance with atmospheric aging of aerosols, Atmos. Chem. Phys., 10, 7267-7283, https://doi.org/10.5194/acp-10-7267-2010, 2010.

Wang, Y., Liu, F., He, C., Bi, L., Cheng, T., Wang, Z., Zhang, H., Zhang, X., Shi, Z., and Li, W.: Fractal Dimensions and Mixing Structures of Soot Particles during Atmospheric Processing, Environ. Sci. Technol. Lett., 4, 487-493, https://doi.org/10.1021/acs.estlett.7b00418, 2017.

Wentzel, M., Gorzawski, H., Naumann, K. H., Saathoff, H., and Weinbruch, S.: Transmission electron microscopical and aerosol dynamical characterization of soot aerosols, J. Aerosol Sci, 34, 1347-1370, https://doi.org/10.1016/S0021-8502(03)00360-4, 2003.

West, J. J., Cohen, A., Dentener, F., Brunekreef, B., Zhu, T., Armstrong, B., Bell, M. L., Brauer, M., Carmichael, G., Costa, D. L., Dockery, D. W., Kleeman, M., Krzyzanowski, M., Künzli, N., Liousse, C., Lung, S.-C. C., Martin, R. V., Pöschl, U., Pope, C. A., Roberts, J. M., Russell, A. G., and Wiedinmyer, C.: "What We Breathe Impacts Our Health: Improving Understanding of the Link between Air Pollution and Health", Environ. Sci. Technol., 50, 4895-4904, https://doi.org/10.1021/acs.est.5b03827, 2016.

Wu, Y., Cheng, T., Liu, D., Allan, J. D., Zheng, L., and Chen, H.: Light Absorption Enhancement of Black Carbon Aerosol Constrained by Particle Morphology, Environ. Sci. Technol., 52, 6912-6919, https://doi.org/10.1021/acs.est.8b00636, 2018.

Xu, L., Zhang, D., and Li, W.: Microscopic comparison of aerosol particles collected at an urban site in North China and a coastal site in Japan, Sci. Total Environ., 669, 948-954, https://doi.org/10.1016/j.scitotenv.2019.03.163, 2019.

You, Y., Renbaum-Wolff, L., Carreras-Sospedra, M., Hanna, S. J., Hiranuma, N., Kamal, S., Smith, M. L., Zhang, X., Weber, R. J., Shilling, J. E., Dabdub, D., Martin, S. T., and Bertram, A. K.: Images reveal that atmospheric particles can undergo liquid–liquid phase separations, Proc. Natl. Acad. Sci. U.S.A., 109, 13188-13193, https://doi.org/10.1073/pnas.1206414109, 2012.

Yuan, Q., Xu, J., Wang, Y., Zhang, X., Pang, Y., Liu, L., Bi, L., Kang, S., and Li, W.: Mixing State and Fractal Dimension of Soot Particles at a Remote Site in the Southeastern Tibetan Plateau, Environ. Sci. Technol., 53, 8227-8234, https://doi.org/10.1021/acs.est.9b01917, 2019.

Zhang, D., Iwasaka, Y., Shi, G., Zang, J., Hu, M., and Li, C.: Separated status of the natural dust plume and polluted air masses in an Asian dust storm event at coastal areas of China, J. Geophys. Res.: Atmos., 110, D06302, https://doi.org/10.1029/2004JD005305, 2005.

Zhang, G., Bi, X., Li, L., Chan, L. Y., Li, M., Wang, X., Sheng, G., Fu, J., and Zhou, Z.: Mixing state of individual submicron carbon-containing particles during spring and fall seasons in urban Guangzhou, China: a case study, Atmos. Chem. Phys., 13, 4723-4735, https://doi.org/10.5194/acp-13-4723-2013, 2013.

Zhang, R., Khalizov, A. F., Pagels, J., Zhang, D., Xue, H., and McMurry, P. H.: Variability in morphology, hygroscopicity, and optical properties of soot aerosols during atmospheric processing, Proc. Natl. Acad. Sci. U.S.A., 105, 10291-10296, https://doi.org/10.1073/pnas.0804860105, 2008.

Zhang, X., Mao, M., Yin, Y., and Wang, B.: Numerical Investigation on Absorption Enhancement of Black Carbon Aerosols Partially Coated With Nonabsorbing Organics, J. Geophys. Res.: Atmos., 123, 1297-1308, https://doi.org/10.1002/2017JD027833, 2018a.

Zhang, Y., Su, H., Ma, N., Li, G., Kecorius, S., Wang, Z., Hu, M., Zhu, T., He, K., Wiedensohler, A., Zhang, Q., and Cheng, Y.: Sizing of Ambient Particles From a Single-Particle Soot Photometer Measurement to Retrieve Mixing State of Black Carbon at a Regional Site of the North China Plain, J. Geophys. Res.: Atmos., 123, 12,778-712,795, https://doi.org/10.1029/2018JD028810, 2018b.

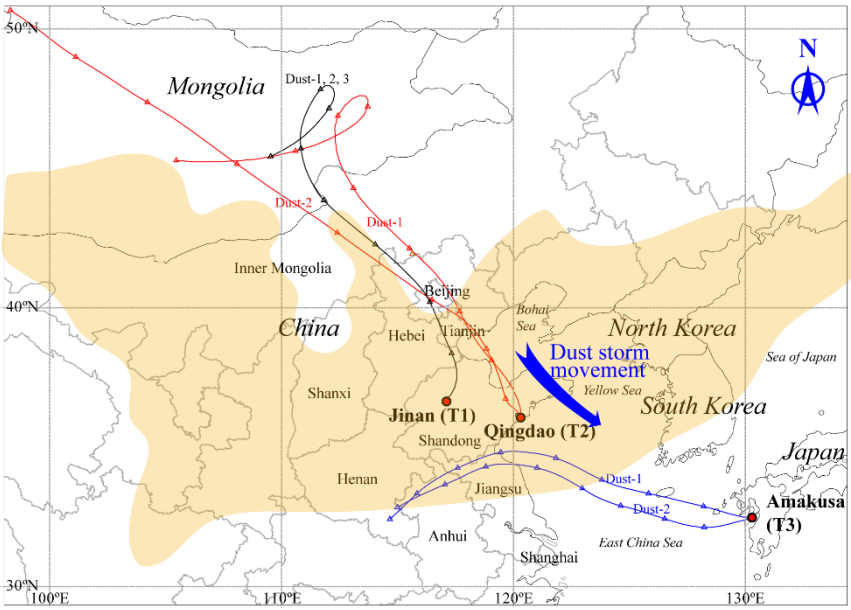

606

607 Figure 1. The locations of the three sampling sites and HYSPLIT forty-eight hour air
608 mass backward trajectories arriving at 1500 m above ground level at T1, T2, and T3
609 sites. The interval between two triangle symbols is six hours. The yellow shadow is
610 derived from Figure S1, which represents the area influenced by the dust storm at 00:00
611 on 2014/03/18 (UTC).

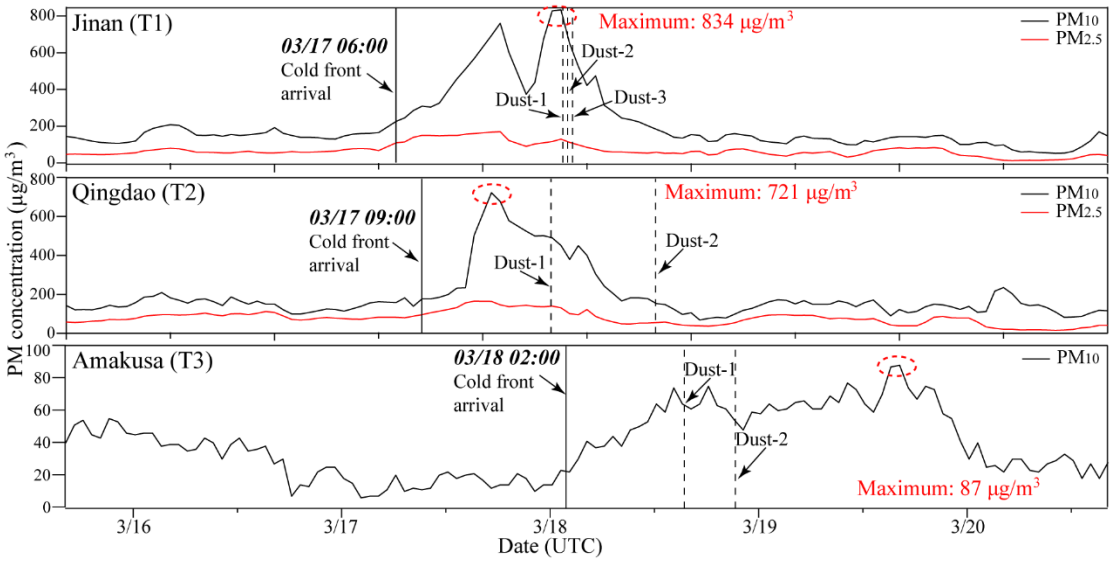

612

613 Figure 2. Time series of PM (particulate matter) concentrations at T1, T2, and T3 during
614 sampling. The cold front arrival times indicate the time when the sampling site starts to
615 be influenced by the dust storm. Data sources: T1 and T2: The Ministry of Ecology and
616 Environment of the People's Republic of China, https://www.aqistudy.cn/; T3: National
617 Institute for Environmental Studies of Japan, https://www.nies.go.jp/igreen/).

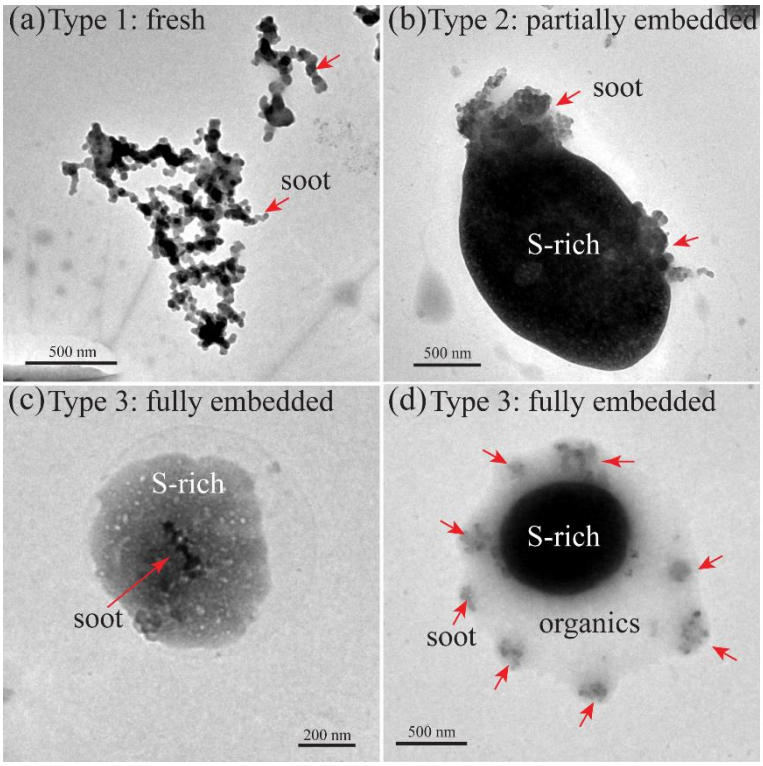

Figure 3. Morphology of soot-bearing aerosol particles: (a) fresh chain-like soot aggregates with no visible coating; (b) partially embedded soot: part of the soot particle was coated by secondary aerosols; (c) fully embedded soot: the whole soot particle was encapsulated by secondary aerosols; (d) a subtype of fully embedded soot: individual soot particles were only embedded in the organic coating on a sulfur-rich particle.

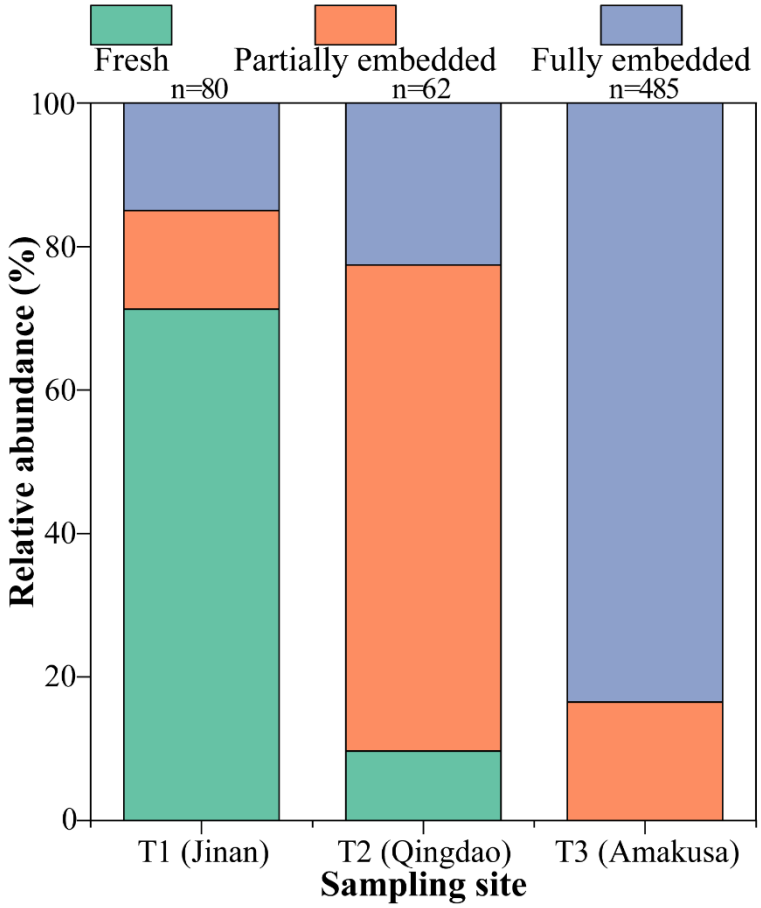

Figure 4. Relative abundance of three types of soot-bearing aerosol particles at the three sampling sites. The number of analyzed soot-bearing particles is shown above the column.

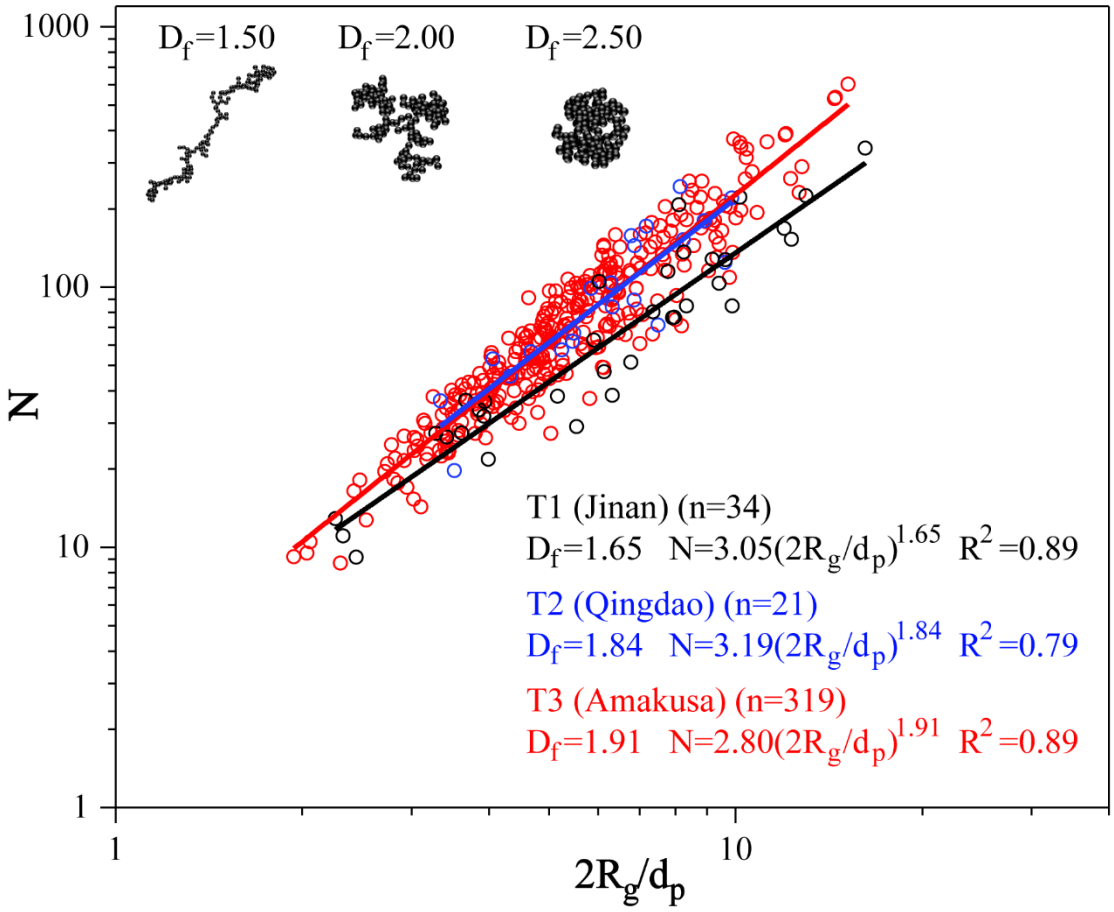

Figure 5. Fractal dimension of soot-bearing particles at the three sampling sites. The parameter n in parentheses represents the total number of soot particles analyzed for each site to calculate D_f and k_g. Three model simulated soot particles with different D_f are presented to represent different soot morphology. The inconsistency of analyzed soot number in Figure 4 and 5 is attributed to the indistinct soot particles in the low-magnification TEM images that can be identified as soot but cannot provide necessary data for D_f analysis.

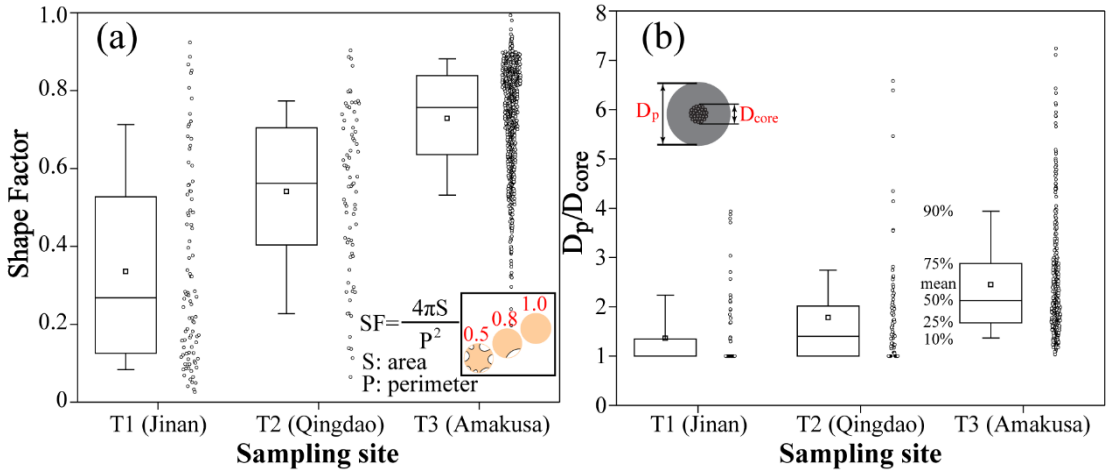

639

640 Figure 6. (a) Shape factor of soot-bearing particles and (b) the particle-to-soot core

641 diameter ratio (D_p/D_{core}) at the three sampling sites.

642

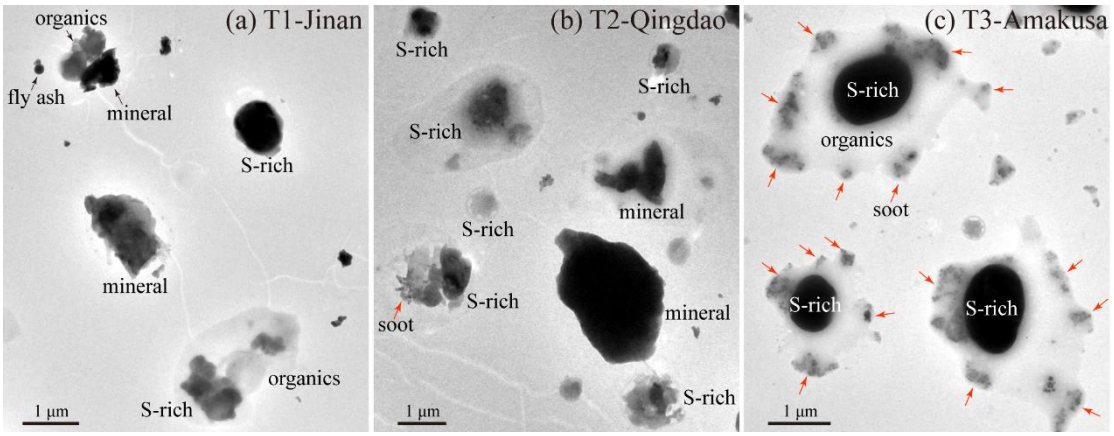

643

644 Figure 7. Low-magnification TEM images at T1, T2, and T3.

645

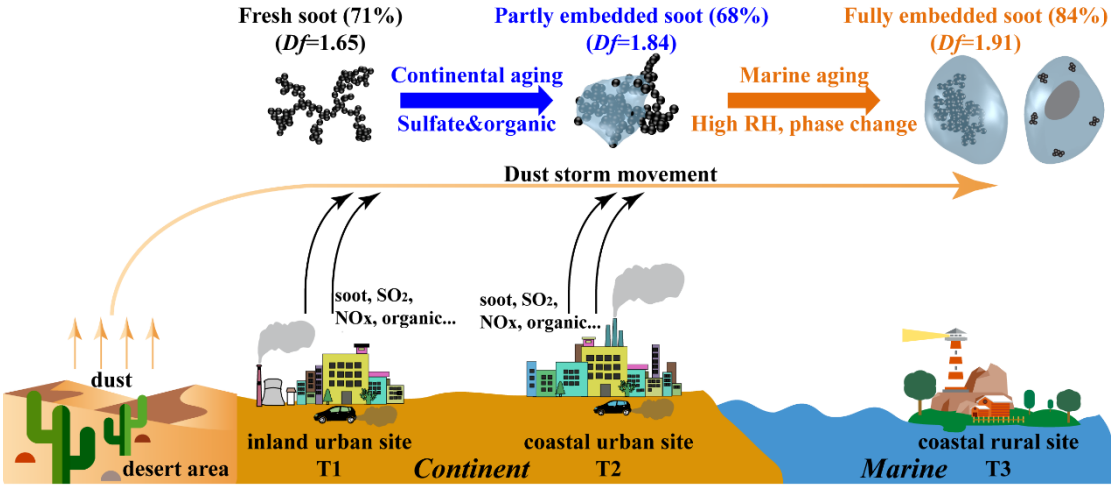

646

647 Figure 8. Schematic diagram showing the evolution of morphology and mixing state of

soot particles along with the movement of an Asian dust storm